Title

Integrative genomic reconstruction reveals heterogeneity in carbohydrate utilization across human gut bifidobacteria

Author list

Aleksandr A. Arzamasov[1], Dmitry A. Rodionov[1], Matthew C. Hibberd[2,3], Janaki L. Guruge[2,3], James E. Kent[1], Marat D. Kazanov[4], Semen A. Leyn[1], Marinela L. Elane[1], Kristija Sejane[5], Annalee Furst[5], Lars Bode[5], Michael J. Barratt[2,3], Jeffrey I. Gordon[2,3], and Andrei L. Osterman[1]

Corresponding authors:

Jeffrey I. Gordon (jgordon@wustl.edu)

Andrei L. Osterman (osterman@sbpdiscovery.org)

Affiliations

[1]Center for Data Sciences, Sanford Burnham Prebys Medical Discovery Institute, 10901 North Torrey Pines Rd, La Jolla, CA 92037, USA

[2]Edison Family Center for Genome Sciences and Systems Biology, Washington University School of Medicine, St. Louis, MO 63110, USA.

[3]Newman Center for Gut Microbiome and Nutrition Research, Washington University School of Medicine, St. Louis, MO 63110, USA.

[4]Faculty of Engineering and Natural Sciences, Sabanci University, Istanbul, 34956, Turkey

[5]Department of Pediatrics, Larsson-Rosenquist Foundation Mother-Milk-Infant Center of Research Excellence (MOMI CORE), and the Human Milk Institute (HMI), University of California San Diego, La Jolla, CA 92093, USA

Abstract

Bifidobacteria are among the earliest colonizers of the human gut and are widely used as probiotics for their health-promoting properties. However, individual responses to probiotic supplementation may vary with strain type(s), microbiota composition, diet, or lifestyle conditions, highlighting the need for strain-level insights into the bifidobacterial metabolism of dietary and host glycans. Here, we systematically reconstructed 68 pathways involved in the utilization of mono-, di-, oligo-, and polysaccharides by analyzing the distribution of 589 curated metabolic functional roles (catabolic enzymes, transporters, transcriptional regulators) in 3083 non-redundant cultured *Bifidobacterium* isolates and metagenome-assembled genomes (MAGs) of human origin. Our analysis uncovered extensive inter- and intraspecies heterogeneity, including a distinct clade within the *Bifidobacterium longum* species capable of metabolizing α-glucans. We also identified isolates of Bangladeshi origin that harbor unique gene clusters implicated in the breakdown of xyloglucan and human milk oligosaccharides. Thirty-eight predicted carbohydrate utilization phenotypes were experimentally validated in 30 geographically diverse *Bifidobacterium* isolates *in vitro*. Our large-scale genomic compendium expands the knowledge of bifidobacterial carbohydrate metabolism and can inform the rational design of probiotic and synbiotic formulations tailored to strain-specific nutrient preferences.

Bifidobacteria are Gram-positive, saccharolytic microorganisms that predominantly inhabit animal gastrointestinal tracts[1]. Multiple *Bifidobacterium* species colonize the human gut throughout life, with dietary carbohydrate intake playing a key role in shaping this process[2]. Breastfeeding fosters the dominance of specific *Bifidobacterium* species within the neonatal gut microbiota due to their evolutionary adaptation to metabolize human milk oligosaccharides (HMOs)[3–5]. Weaning drives a gradual succession of bifidobacterial taxa from those tuned for HMO utilization to those more adapted to foraging dietary glycans (oligo- and polysaccharides) of plant origin[6–8].

Geographic and cultural dietary differences also profoundly influence the bifidobacterial composition of neonatal microbiotas. For example, *Bifidobacterium longum* subsp. *infantis* (*Bl. infantis*), a specialist HMO utilizer, constitutes up to 90% of the gut microbial composition of healthy breastfed infants from non-Westernized populations[9–11]. Infants from Westernized populations often lack *Bl. infantis* and instead harbor less proficient HMO utilizers such as *Bifidobacterium longum* subsp. *longum* (*Bl. longum*), *Bifidobacterium breve*, and *Bifidobacterium pseudocatenulatum*; this appears to be due to a combination of lifestyle and cultural factors[9,12,13].

Despite these differences, the predominance of bifidobacteria in gut communities is associated with multiple health benefits, particularly in infancy. Bifidobacterial fermentation products, lactate and acetate, can inhibit pathogen colonization[14,15] and serve as substrates for cross-feeding among microbial community members[16,17]. Additionally, multiple *Bifidobacterium* species produce aromatic lactic acids modulating the immune system[18,19]. These beneficial traits underpin the widespread use of bifidobacterial strains as probiotics[20–23], often supplemented with complementary prebiotics to facilitate engraftment[23,24].

Further development is needed to rationally select probiotic strains and prebiotic glycans tailored for different populations. For instance, a probiotic *Bl. infantis* strain did not durably engraft in the microbiota of malnourished Bangladeshi infants whose diets were low in breastmilk compared to complementary foods[23]. Moreover, strains isolated from children in this population may harbor distinctive genomic adaptations for metabolizing glycans common in weaning diets[23]. Thus, strain-level insights into bifidobacterial carbohydrate metabolism, especially in understudied populations, may be instrumental in developing locally adapted pro- and synbiotics.

Genomics-based approaches, including the analysis of Carbohydrate Active Enzymes (CAZymes) repertoires[7,25–27], genotype-to-phenotype matching[28–30], and genome-scale metabolic models[31–33], have been used to predict the carbohydrate utilization capabilities of bifidobacteria. However, functional gene annotations, particularly for glycan transporters, remain insufficiently curated and integrated into metabolic reconstructions[34]. In addition, current genomic resources may not fully capture the strain-level diversity within the *Bifidobacterium* genus.

We employed a combination of curated metabolic reconstruction and machine learning to map 68 carbohydrate utilization pathways across 263 reference and 2,820 additional *Bifidobacterium* genomes by analyzing the representation of 589 functional roles (catabolic enzymes, CAZymes, transporters, and transcriptional regulators). Thirty-eight predicted glycan utilization phenotypes were validated *in vitro* using 30 diverse strains. Our findings reveal remarkable inter- and intraspecies variability, including a distinct *Bifidobacterium longum* clade that metabolizes α-glucans and Bangladeshi strains carrying unique gene clusters for plant hemicellulose and HMO metabolism. These insights establish a genomic framework for predicting glycan utilization networks across *Bifidobacterium* lineages and support the development of targeted pre-, pro-, and synbiotics.

RESULTS

Curated metabolic reconstruction from reference genomes

The curated reconstruction encompassed a non-redundant reference set of 263 *Bifidobacterium* genomes of cultured isolates, including 19 newly sequenced genomes of Bangladeshi strains (**Supplementary Tables 1**,**2**). To refine taxonomic assignments, we first constructed a maximum-likelihood phylogenetic tree based on 487 core genes identified through a pangenome analysis (**Supplementary Fig. 1**). Additional pairwise average nucleotide identity (ANI) comparisons for 39 genomes allowed us to delineate the within-species structure of *Bifidobacterium longum* and *Bifidobacterium catenulatum* species (**Extended Data Fig. 1**; *Supplementary Note 1*). Overall, the reference set spanned 19 species and subspecies (**Supplementary Table 1**).

We leveraged a subsystem-based comparative genomics framework[35] to reconstruct carbohydrate utilization pathways and predict associated metabolic phenotypes (**Fig. 1a**). We first mined 222 publications to identify 433 orthologous groups of carbohydrate utilization genes, whose encoded proteins were either experimentally characterized in bifidobacteria (210 metabolic functional roles), shared significant sequence similarity with proteins characterized in other microbial taxa (80 roles), or were previously assigned putative functions (143 roles). Genomic context analysis, including *in silico* transcriptional regulon reconstruction (*Supplementary Notes 2-3*), enabled tentative functional predictions for 156 additional gene groups involved in glycan metabolism. The resulting curated set of 589 roles — comprising 235 components of glycan-specific transporters, 197 catabolic CAZymes, 72 downstream catabolic enzymes, and 85 transcription factors — was used to functionally annotate 39,589 of 541,418 protein-coding genes across 263 reference genomes (**Supplementary Tables 4**,**8**). Manual curation improved 76.6% and 69% of annotations over Prokka and EggNOG-mapper, respectively, including more than 90% of annotations for transporters and transcriptional regulators (**Fig. 1b)**. The metabolic reconstruction also captured 82.2% of catabolic CAZymes identified by dbCAN (**Fig. 1c**).

The genome-wide distribution of genes assigned to 589 functional roles was used to reconstruct 68 catabolic pathways: 18 for monosaccharides and their derivatives (sugar alcohols and acids), 39 for di- and oligosaccharides, and 11 for polysaccharides (**Supplementary Table 5**). To link gene conservation patterns with metabolic phenotypes, we first established rules that

define genomic signatures distinguishing metabolic pathway variants (*Methods*; **Extended Data Fig. 2**; **Supplementary Table 6**). Each pathway variant was then converted into a binary phenotype, classifying strains as predicted utilizers ("1") or non-utilizers ("0") of specific carbohydrates. These assignments formed a Binary Phenotype Matrix (BPM), summarizing the predicted utilization profiles of 263 reference *Bifidobacterium* strains spanning 68 glycans (**Supplementary Table 7**). To evaluate the robustness of our reconstruction, we compared predicted phenotypes with *in vitro* growth data for 33 strains from previous studies[8,28,36], yielding 94% accuracy (**Supplementary Table 17a–d**).

Automated pathway prediction across large genomic datasets

We utilized the metabolic reconstruction for 263 reference *Bifidobacterium* genomes to analyze the representation of glycan utilization pathways in an additional set of 2,820 non-redundant genomes (**Supplementary Table 3**). This set included 364 isolate genomes and 2,456 high-quality metagenome-assembled genomes (MAGs) with completeness ≥97 % and contamination ≤3%. Twelve genomes represented four species absent from the reference collection, and nine were from Bangladeshi and Malawian strains isolated in previous studies[37–39] and sequenced in this work (**Supplementary Table 1**). We used annotated protein sequences of reference strains to assign functions to a subset of 419,055 protein-coding genes in the 2,820 genomes. These functional annotations, combined with the reference BPM, were used to train a random forest model that predicted the presence of 68 reconstructed carbohydrate utilization pathways (*Methods*; **Fig. 1a**; **Supplementary Tables 9**,**10**).

Interspecies diversity in glycan utilization

The BPMs for 263 reference and 2,820 additional genomes were merged to assess the distribution of glycan utilization pathways across the *Bifidobacterium* genus. Non-metric multidimensional scaling (NMDS) of the Hamming distance matrix derived from the BPM of 3,083 genomes revealed grouping by species/subspecies, with taxonomy explaining 91% of the variation (PERMANOVA $R^2 = 0.91$, $P = 0.001$; **Fig. 2a**). A significant dispersion effect ($F = 81.06$, $P= 0.001$) indicated that strain-level variability in pathway representation differed across taxa, likely influencing the separation.

We observed significant differences in predicted phenotypic richness (total number of predicted carbohydrate utilization pathways) between taxa, including phylogenetically close subspecies sharing over 95% ANI (Poisson generalized linear model, $p < 2.2 \times 10^{-16}$; **Fig. 2b**). For example, *Bifidobacterium catenulatum* subsp. *catenulatum* (*Bc. catenulatum*) had significantly lower phenotypic richness than subspecies *kashiwanohense* (*Bc. kashiwanohense*) and *kashiwanohense_A* (*Bc. kashiwanohense_A*) due to the absence of utilization pathways for fucosylated HMOs (e.g., 2'- and 3-fucosyllactose, 2'FL/3FL), and certain plant oligosaccharides (e.g., beta-mannose oligosaccharides, bMnOS) in >95% of genomes (**Extended Data Fig. 3**; *Supplementary Note 4*).

Pathways for glucose (Glc), galactose (Gal), fructose (Fru), lactose (Lac), and galactooligosaccharide (GOS) utilization were identified in over 98% of analyzed genomes, defining the core catabolic potential of human-colonizing bifidobacteria (**Fig. 2c**). Pathways for sucrose (Scr), maltose (Mal), malto- and isomaltooligosaccharide (MOS and IMO), melibiose (Mel), raffinose-family oligosaccharide (RFO), and short-chain fructooligosaccharide (scFOS) metabolism were encoded in over 84% of genomes, indicating broad conservation across most species, except *Bifidobacterium bifidum.* Other pathways showed more sporadic distribution patterns, reflecting species-level adaptations for metabolizing dietary glycans of different origins and structures. For example, *B. bifidum* exhibited a notable specialization towards the metabolism of host mucin *O*-glycans, HMOs, and their degradation products lacto-*N*-biose (LNB), galacto-*N*-biose (GNB), and *N*-acetyl-D-glucosamine (GlcNAc) — consistent with prior reports[40] (**Fig. 2c**). At the same time, most *B. bifidum* genomes lacked complete pathways for utilizing plant-derived mono-, di-/oligo- and polysaccharides. Other bifidobacteria, including the specialist HMO utilizer *Bl. infantis,* were more versatile in their predicted glycan utilization profiles, although the pathways for plant polysaccharide degradation were generally underrepresented compared to those for their mono- and oligosaccharide components (**Fig. 2c**).

Hierarchical clustering of the BPM for 263 reference genomes showed a moderate correlation with core-gene phylogeny (cophenetic correlation = 0.58, permutation test, $p < 0.001$; **Supplementary Fig. 2**), indicating incomplete concordance between predicted glycan utilization capabilities and phylogenetic relatedness. For example, the predicted phenotypic profiles of *Bl. infantis* and *Bl. longum*, two phylogenetically related subspecies within the *B. longum* species, were markedly different. The representation of glycan utilization pathways in *Bl. infantis* more

closely resembled that of *B. breve* — a more distantly related species inhabiting the neonatal human gut. Given the importance of *B. longum* in infant microbiota development, we next conducted a more focused analysis of pathway variability within this heterogeneous species.

Diversity of glycan metabolism within the *B. longum* species

The *B. longum* species comprises multiple subspecies distinguished by phylogeny and specific phenotypic traits[26,41–43]. Our phylogenomic and ANI analyses clustered *B. longum* genomes into three clades matching previously described subspecies — *infantis* (*Bl. infantis*), *longum* (*Bl. longum*), *suis* (*Bl. suis*) — and a distinct clade hereafter referred to as *Bl. nov.* (**Extended Data Fig. 1a**; **Supplementary Fig. 1**; *Supplementary Note 1*). *Bl. nov.* exhibited significantly lower predicted phenotypic richness than other subspecies (**Fig. 2b**), lacking pathways for LNB/GNB, *N*-glycan, HMO, and T-antigen (Tan) metabolism (**Fig. 2c**; *Supplementary Note 5*). Conversely, only *Bl. nov.* genomes encoded extracellular amylopullulanase ApuB (GH13_14_32), a bifunctional glycoside hydrolase (GH) cleaving both α-1,4 and α-1,6-glycosidic bonds in soluble starch (ST) and pullulan (PUL)[44], and a pathway for difructose dianhydride (DFA) metabolism[45]. These findings suggest that *Bl. nov.* has a reduced capacity to metabolize host-derived glycans but can degrade α-glucans of plant and fungal origin.

Comparative analysis of carbohydrate utilization pathways revealed stark differences between *Bl. infantis* and *Bl. longum* (**Fig. 2c**). Consistent with previous studies, *Bl. infantis* genomes were distinguished by the presence of H1[46] and FL1/2[4] gene clusters, which enable the utilization of lacto-*N*-neotetraose (LNnT), 2'FL, 3FL, lactodifucotetraose (LDFT), lacto-*N*-fucopentaose I (LNFP I), and sialylated HMOs (SHMOs; **Supplementary Tables 7–10**). Predicted HMO utilization potential of *Bl. longum* was more limited: 35% of genomes encoded an extracellular lacto-*N*-biosidase (LnbX; GH136) that cleaves lacto-*N*-tetraose (LNT) and LNFP I[47], and only 2.3% harbored a gene cluster for intracellular utilization of 2'/3FL, LDFT, and LNFP I[48,49]. Beyond HMO metabolism, *Bl. infantis* exclusively encoded utilization pathways for metabolizing glucuronate (GlcA), inositol (Ino), and gluconate (Gco) in 63%, 48%, and 23% of genomes, respectively (**Extended Data Fig. 4a,b,d,e**; *Supplementary Note 3*) *Bl. longum* genomes, by contrast, commonly encoded pathways for L-arabinose (Ara), α/β-arabinooligosaccharides (aAOS/bAOS), type II arabinogalactan (AGII), arabinan (AR),

arabinoxylan (AX), and host- or plant-derived *O*-glycans (Tan, HRGP) (**Fig. 2c**). These findings illustrate an ecological divergence between *Bl. infantis* and *Bl. longum* shaped by their respective adaptations to thrive on milk glycans during breastfeeding versus plant-derived carbohydrates after weaning.

Predicted glycan utilization profiles within the *Bl. suis* group were highly heterogeneous. Most genomes encoded a set of pathways similar to that of *Bl. longum*, yet more frequently included pathways for *N*-acetylneuraminic acid (Neu5Ac; 44% vs. 2%), L-fucose (Fuc; 61% vs. 1.7%), and fucosylated HMOs (2'/3FL, LDFT, LNFP I; 56% vs. 2.3%), while lacking extracellular α-L-arabinofuranosidases required for AX degradation[50,51] (**Fig. 2c**; **Supplementary Tables 8**,**10**). In contrast, the Bangladeshi strain Bg131.S11_17.F6 exhibited a *Bl. infantis*-like pathway profile (**Supplementary Figure 3**), carrying the H1 gene cluster for the utilization of multiple HMOs but lacking pathways for arabinose-containing glycans (e.g., Ara, aAOS, AGII). Consequently, this strain was predicted to utilize more distinct HMO structures (e.g., LNnT, SHMOs) than other Bangladeshi *Bl. suis* strains, while having a reduced capacity for plant glycan metabolism. Analysis of 10 additional *Bl. suis* genomes of animal origin confirmed the uniqueness of the Bg131.S11_17.F6 strain and further underscored the phenotypic heterogeneity within this group (**Extended Data Fig. 5**; *Supplementary Note 5*). Collectively, these findings reveal pronounced differences in carbohydrate utilization across *B. longum* subspecies and underscore pervasive strain-level heterogeneity within each clade, a phenomenon explored in detail below.

Strain-level heterogeneity of glycan metabolism

Beyond interspecies differences, we observed extensive strain-level variability in predicted carbohydrate utilization capabilities. Of the 68 reconstructed pathways, 66 exhibited variability within at least one taxonomic group (**Fig. 2c**; **Supplementary Tables 7**,**9**). The genomic differences driving this heterogeneity ranged from individual genes encoding extracellular GHs enabling polysaccharide degradation to multi-gene clusters comprising up to 20 genes encoding complete metabolic pathways (**Supplementary Table 8**). In contrast, biosynthetic pathways for essential metabolites, such as amino acids and B vitamins, were largely conserved. A few exceptions included riboflavin (B2) biosynthesis, which varied across

Bl. suis and *Bc. kashiwanohense_A*, and thiamine (B1) and niacin (B3) biosynthesis in *Bifidobacterium adolescentis* (**Extended Data Fig. 6**; **Supplementary Table 11**).

The observed heterogeneity suggests that while most *Bifidobacterium* taxa follow general ecological strategies centered on the utilization of specific core glycans, individual strains can exhibit substantial metabolic tuning. For instance, *Bl. infantis* Bg064.S07_13.C6 harbored pathways for xylooligosaccharide (XOS) and long-chain fructooligosaccharide (lcFOS) utilization, suggesting an enhanced capacity to metabolize dietary plant glycans compared to most other *Bl. infantis* strains (**Supplementary Fig. 3**). Conversely, several *B. adolescentis* isolates carried pathways for the utilization of LNB/GNB, *N*-glycans (strains AF96-10M2bTA, UN03-88), and fucosylated HMOs (M56B_1C3), highlighting the presence of traits characteristic of infant-adapted taxa in a species commonly associated with the adult gut (**Supplementary Tables 9,10**). Additional examples of notable strain-specific genomic features related to carbohydrate utilization were found in Bangladeshi isolates and are detailed below.

Unique glycan utilization features of Bangladeshi strains

Our previous study identified distinctive genomic features of Bangladeshi *Bl. infantis* strains related to *N*-glycan and beta-glucoside catabolism[23]. Here, we identified a distinct gene cluster (*xgl*) in *Bc. kashiwanohense* Bg42221_1E1 and *Bc. kashiwanohense_A* Bg42221_1D3, two isolates from a Bangladeshi infant (**Fig. 3a**). This cluster encoded multiple GHs (families 3, 5_4, 29, 31, 42, 43_12), an unclassified carbohydrate esterase (CE), a β-glucoside kinase, and an ABC transport system, which together may catabolize plant hemicelluloses such as xyloglucans (XGL). The reconstructed XGL pathway involved the hydrolysis of the XGL backbone to oligosaccharides by extracellular endo-β-1,4-glucanase Xgl5A (GH5_4), which shares catalytic and glycan-binding residues with xyloglucanase PpXG5 from *Paenibacillus pabuli* XG5[52] (**Extended Data Fig. 7a**). Released oligosaccharides would be imported into the cell and degraded sequentially to individual monosaccharides and cellobiose by the coordinated action of GHs and CEs via a mechanism similar to that described in *Ruminiclostridium cellulolyticum*[53] (**Fig. 3b**). Regulon reconstruction of XglT, a putative TetR-family transcription factor, suggested potential co-regulation of the *xgl* cluster and *cbpA*, which encodes a GH94-family cellobiose phosphorylase (**Fig. 3a-c**; **Supplementary Table 19**). The *xgl* cluster was identified in only 3 of

110 studied *B. catenulatum* genomes but was conserved in *Bifidobacterium dentium* and *Bifidobacterium tsurumirense*.

Another gene cluster, unique to *Bc. kashiwanohense* Bg42221_1E1, contained orthologs of H1 cluster HMO utilization genes from *Bl. infantis* and the "outlier" Bangladeshi *Bl. suis* Bg131.S11_17.F6 strain (**Fig. 4a**). The H1 variant identified in Bg42221_1E1 encoded two ABC transporters, one of which (HmoABC) is likely involved in the uptake of LNnT and other type II HMO structures[54]. Additionally, this cluster encoded orthologs of characterized β-*N*-acetylglucosaminidase (GH20), two α-fucosidases (GH29 and GH95), and α-sialidase (GH33), which mediate intracellular HMO hydrolysis[55–57], along with downstream catabolic pathways for GlcNAc and Fuc. Regulon reconstruction suggested the potential transcriptional regulation of H1 cluster genes in *Bc. kashiwanohense* Bg42221_1E1 by NagR, a GlcNAc-responsive ROK-family repressor[58] (**Fig. 4a**; **Supplementary Table 19**).

Other notable features of Bangladeshi *Bifidobacterium* isolates included a putative D-galactonate utilization pathway found exclusively in *B. breve* Bg41721_1C11 (**Extended Data Fig. 4d,e**; *Supplementary Note 3*). This strain, along with *B. breve* Bg131.S11_D6, also lacked the *nan* gene cluster, which encodes a well-characterized Neu5Ac catabolic pathway[59] (**Extended Data Fig. 4f,g**). This absence of the *nan* cluster in these two strains was unexpected, given its previously reported broad conservation in *B. breve* genomes[29,59] and its established role in utilizing Neu5Ac via cross-feeding on sialylated HMOs and mucin *O*-glycans degraded by *B. bifidum*[59,60].

These results demonstrate that Bangladeshi *Bifidobacterium* strains carry unique adaptations for metabolizing dietary plant polysaccharides and HMO, while lacking pathways conserved in well-characterized strains. These traits may reflect strain-level adaptation to the diet and lifestyle of Bangladeshi children. We next investigated whether broader patterns of bifidobacterial carbohydrate utilization are associated with host age and lifestyle across diverse human populations.

Associations between pathway profiles and lifestyle

We examined the enrichment of glycan utilization pathways in *Bifidobacterium* genomes from different populations based on: (i) host age/stage of gut microbiota maturation (< 3 years: infant/transitional; ≥ 3 years: adult-like), and (ii) host lifestyle ("Westernized" vs. "non-

Westernized" as defined in Pasolli et al.[61]). Host glycan utilization pathways (e.g., for HMO) were enriched in genomes from the "age < 3" group, whereas plant glycan utilization pathways were more prevalent in adult-associated (≥ 3 years) genomes across both lifestyle groups (Fisher's exact test, $P_{adj} \leq 0.01$; **Extended Data Fig. 8a,b**). Within the "age < 3" group, 14 pathways (11 for plant glycans) were enriched in the Westernized group and 24, including 11 for HMOs and their constituent blocks LNB, Neu5Ac, and Fuc in the non-Westernized group (**Extended Data Fig. 8c**). These differences likely stem from the uneven taxonomic distribution of species and subspecies across Westernized and non-Westernized microbiota. For example, pathways enriched in the non-Westernized group were associated with *Bl. infantis*, a taxon more prevalent in that group (odds ratio = 4.98, 95% CI: 3.24–7.51, Fisher's exact test, $P = 1.82\times10^{-11}$).

Within taxa, pathways for sorbitol, mannitol (Stl and Mtl), lcFOS, and pectic galactan (PG) metabolism were significantly enriched in Westernized *Bl. infantis* genomes (**Extended Data Fig. 8d**). The Stl and lcFOS utilization pathways were also enriched in Westernized *B. adolescentis* genomes, and the PG pathway was enriched in Westernized *Bl. longum* genomes. Conversely, non-Westernized *B. breve* genomes were enriched for melezitose (Mlz) and 1,2-β-oligoglucan utilization pathways but more frequently lacked the Neu5Ac pathway. These findings underscore how lifestyle-driven ecological pressures shape glycan utilization strategies among bifidobacteria. We next tested carbohydrate utilization phenotypes in representative isolates to validate predictions from the reconstruction framework.

Growth-based validation of predicted glycan utilization

To experimentally test *in silico* carbohydrate utilization predictions, we conducted *in vitro* growth assays on 30 geographically diverse *Bifidobacterium* strains (15 Bangladeshi, 8 Malawian, 5 US, two European). Growth was tested on 43 substrates corresponding to 38 predicted glycan utilization phenotypes: 13 monosaccharides and derivatives, 18 di-/oligosaccharides, and 7 polysaccharides (**Fig. 5a**). Strains were cultured in a sugar-free De Man-Rogosa-Sharpe (MRS-AC) medium[4,58] supplemented with the test substrate (5-10 mg/mL), and growth was defined using strain-specific OD_{600} thresholds (*Methods*; **Supplementary Fig. 4**). Growth outcomes were compared with predictions derived from manual curation (20 strains) or the automated pipeline (10 strains; **Fig. 5b**).

Prediction accuracy was similar for both approaches: 95 and 94%, respectively, with Matthews correlation coefficients of 0.9 and 0.89 (**Supplementary Table 17e,f**). False negative predictions (growth despite predicted non-utilization) likely stemmed from incomplete knowledge about monosaccharide and HMO transporters. For example, *Bl. suis* Bg131.S11_17.F6 grew on 2'FL despite lacking known 2'FL transporter genes[4,5] (**Supplementary Table 8**). Some false positive predictions (predicted utilization but no growth) may have resulted from gene disruptions, such as a premature stop codon in the *gltA* gene in *B. pseudocatenulatum* LFYP29, which likely impaired the LNT transport function.

As predicted, *Bl. nov.* LFYP82 was the only *B. longum* strain to grow on ST and PUL (**Fig. 5a**). We also validated strain-specific utilization of short- and long-chain fructooligosaccharides (scFOS and lcFOS), XOS, and GlcA in *Bl. infantis* (**Fig. 5b; Extended Data Fig. 4c**). Similarly, while two *B. breve* strains grew on mannotriose (bMnOS), none grew on konjac glucomannan (bMAN), in contrast to *B. dentium* LFYP24 and *Bifidobacterium scardovii* JCM 12489, which harbored extracellular endo-β-1,4-mannanases (**Extended Data Fig. 7e-g**; *Supplementary Note 2*).

We further validated several unusual glycan utilization traits predicted in isolates from Bangladesh and Malawi. *Bc. kashiwanohense* Bg42221_1E1 and *Bc. kashiwanohense_A* Bg42221_1D3, both carrying the *xgl* cluster, grew in the medium supplemented with tamarind XGL (**Fig. 3d**). Bangladeshi *B. breve* isolates lacking the Neu5Ac utilization pathway (Bg41721_1C11 and Bg131.S11_D6) failed to grow on Neu5Ac, unlike other tested *B. breve* strains (**Extended Data Fig. 4h**). Finally, consistent with our prediction, *B. adolescentis* M56B_1C3 grew on 2'FL, highlighting the previously unrecognized capacity of this species (**Fig. 5a**).

Glycoprofiling of HMO utilization

The H1 cluster in *Bl. infantis* is believed to enable the metabolism of multiple HMOs[46], though the precise range of structures cannot be confidently predicted due to limited understanding of the functions of individual transporter genes. Given the presence of homologous H1 clusters in *Bl. suis* Bg131.S11_17.F6 and *Bc. kashiwanohense* Bg42221_1E1, we compared their HMO utilization with that of (i) two *Bl. infantis* strains, (ii) phylogenetically related strains carrying a fucosylated HMO utilization gene cluster (FHMO) instead of H1 (*Bl.*

suis Bg41121_2E1 and *Bc. kashiwanohense_A* Bg42221_1D3; **Fig. 4a**), and (iii) distantly related strains predicted to have weak (*Bl. longum*, *B. breve*) or minimal (*Bl. nov.* and *B. pseudocatenulatum*) HMO utilization capacity.

Strains with the H1 cluster reached the highest optical densities when grown in MRS-AC supplemented with an HMO mixture isolated from pooled human milk (**Fig. 4b**). HPLC-based glycoprofiling of culture supernatants revealed that these strains consumed 72-86% of total HMOs by 24h, including multiple fucosylated and sialylated structures (**Fig. 4c**; **Extended Data Fig. 9**). However, *Bl. suis* Bg131.S11_17.F6 and *Bc. kashiwanohense* Bg42221_1E1 did not efficiently utilize 2'FL, the most abundant species in the mixture, in line with the absence of characterized 2'FL transporters. In contrast, strains carrying the FHMO cluster preferentially metabolized fucosylated HMOs, completely depleting 2′FL while exhibiting limited utilization of sialylated structures. Among H1- and FHMO-cluster negative strains, *Bl. longum* Bg115.S08_3A11 depleted LNT, LNnT, LNFP I, LNFP III, LNH, and FLNH likely via partial extracellular degradation by β-galactosidase and lacto-*N*-biosidase, whereas *B. breve* Bg155.S08_4F7 metabolized LNT and LNnT intracellularly (**Supplementary Fig. 5**). *Bl. nov.* LFYP82 failed to efficiently utilize any tested HMOs, consistent with lineage-specific loss of relevant genes. Principal component analysis of growth and HMO utilization data separated strains with H1 and FHMO clusters from each other and all others (**Fig. 4d**). These findings provide the experimental evidence that *Bc. kashiwanohense* and *Bl. suis* strains carrying the H1 cluster exhibit HMO utilization patterns comparable to *Bl. infantis*, and highlight how variation in HMO utilization gene clusters drives metabolic divergence among closely related *Bifidobacterium* strains.

Transcriptional profiles of glycan utilization in *Bc. kashiwanohense*

We used RNA-seq to test regulon predictions and pathway assignments in *Bc. kashiwanohense* Bg42221_1E1, which harbors both *xgl* and H1 gene clusters. Transcriptomic comparison of cultures grown in MRS-AC-XGL vs. MRS-AC-Lac revealed strong induction (100-550 fold) of most *xgl* genes and *cbpA*, supporting their co-regulation by XglT and a shared role in XGL metabolism (**Fig. 3a,e**; **Supplementary Table 21a**). Genes involved in xylose, XOS/AXOS, xylan, and AX metabolism showed moderate upregulation (4-30 fold), likely in response to intracellular xylose release, which may serve as a transcriptional effector of predicted

transcriptional repressors XylR (ROK family) and XosR (LacI family; **Extended Data Fig. 7b,c**; **Supplementary Table 19**; *Supplementary Note 2*)[62]. Next, we compared the transcriptomes of *Bc. kashiwanohense* Bg42221_1E1 grown in MRS-AC-LNT and MRS-AC-Lac. All H1 cluster genes except *nanA2* and *nanH2* were significantly upregulated in the presence of LNT (**Fig. 4e; Supplementary Table 21b**), consistent with the proposed regulation by NagR, a GlcNAc-responsive repressor implicated in the control of HMO utilization in bifidobacteria[58]. Overall, the observed transcriptomes suggest that the regulatory networks of this strain are adapted for foraging on mixtures of HMOs and plant oligo- and polysaccharides.

Our large-scale genomic and experimental analyses pinpoint ecological differences between glycan foraging strategies within *Bifidobacterium* that reflect species-level evolutionary adaptation to different habitats (e.g., infant gut vs. adult gut) and dietary carbohydrate composition. The results also underscore considerable strain-level variability, likely shaped by host lifestyle and local dietary exposures.

DISCUSSION

The ability to metabolize dietary glycans is central to bifidobacterial fitness in the human gut, with 8–12% of their gene content dedicated to carbohydrate metabolism[63]. Understanding this process has fundamental and translational relevance, including for the development of pro- and prebiotics. While interspecies differences in glycan preferences within bifidobacteria are well documented[25,64,65], within-species variability, particularly in populations from low- and middle-income countries, remains understudied. The growing availability of *Bifidobacterium* genomes, driven by culturomics[66–69] and metagenomics[70–75], provides an opportunity to address this gap. However, accurately predicting carbohydrate utilization phenotypes from genomic data remains challenging due to imprecise functional annotations (particularly of glycan transporters) generated by widely-used pipelines, as well as incomplete representation of metabolic pathways in public databases[34,76,77]. To address this gap, we reconstructed 68 carbohydrate utilization pathways encoded in 3,083 *Bifidobacterium* genomes and MAGs and validated 38 predicted phenotypes *in vitro*, with an overall accuracy exceeding 94%. Several false-negative predictions for specific mono- and oligosaccharides, including HMOs, suggest the existence of yet uncharacterized glycan transport mechanisms in bifidobacteria.

Our analysis revealed taxon-specific distribution of glycan utilization pathways, reflecting the adaptation of *Bifidobacterium* species and subspecies to distinct ecological niches, such as the infant and adult gut, and expanding on earlier observations[25,30,64,65]. For instance, we identified a distinct clade within the *B. longum* species (*Bl. nov*.) specialized in metabolizing plant and fungal α-glucans but incapable of utilizing host glycans such as LNB, GNB, and HMOs. As most *Bl. nov*. genomes originated from infants in Westernized populations, the unique glycan preferences of this clade might reflect an adaptation to differences in early-life diet and feeding practices. However, certain pathways, such as raffinose utilization, were widely conserved. A recent study demonstrated that raffinose metabolism supports *B. breve* colonization and persistence in *in vivo*[19], suggesting that conservation of this pathway across bifidobacterial lineages may promote their persistence and transmission beyond infancy.

Another important observation was extensive strain-level variability driven by accessory genome differences ranging from single genes to gene cassettes encoding entire carbohydrate utilization pathways. Particularly notable was the heterogeneity of *Bl. suis* isolates of Bangladeshi origin. Similar strains were recently predicted to utilize HMOs and plant fibers based on the analysis of CAZyme repertoires and reclassified as *B. longum* subsp. *iuvenis*[7,43]. Our analysis revealed nuanced metabolic differences within this clade, suggesting the presence of two distinct "ecotypes". The first, exemplified by strain Bg131.S11_17.F6, metabolizes a wide array of HMOs — including LNT, LNnT, long-chain fucosylated, and sialylated species — but not arabinose and plant polysaccharides, mimicking the glycan preferences of *Bl. infantis*. The second ecotype, represented by strain Bg41121_2E1, preferentially utilizes fucosylated HMO structures, including the abundant 2'FL, but can metabolize arabinose-containing oligo- and polysaccharides, phenotypically resembling previously characterized *Bl. longum* strains SC596 and MC10007[48,49]. These distinct and complementary strategies suggest ecological specialization within the *Bl. suis* group, potentially linked to diet and weaning status.

Further within-species variability is illustrated by Bangladeshi isolates carrying unique gene clusters. One notable example was the *xgl* cluster identified in *Bc. kashiwanohense* Bg42221_1E1 and *Bc. kashiwanohense_A* Bg42221_1D3 strains isolated from the same infant. This cluster enables xyloglucan degradation, a capability previously suggested only for *Bifidobacterium* species inhabiting captive marmosets[78]. Another unexpected discovery was the presence of an H1 cluster variant in *Bc. kashiwanohense* Bg42221_1E1, formerly considered to

be exclusive for *Bl. infantis*[46] and rare Bangladeshi *Bl. suis* group strains[7,23]. Although the precise substrate-specificities of transporters encoded by H1 cluster remain to be characterized, our data confirm that its presence enables the utilization of major HMOs found in human milk. *Bc. kashiwanohense* strains have been shown to metabolize fucosylated HMOs (2'FL and LNFP I) and plant hemicelluloses (xylan and arabinoxylan)[8]. Our findings expand the catabolic potential of *Bc. kashiwanohense* to xyloglucan and a broader range of HMOs (LNT, LNnT, and sialylated HMOs). These results indicate an evolutionary adaptation of Bangladeshi strains to thrive in the microbiota of weaning children, whose diets may combine breast milk with complementary foods rich in plant polysaccharides.

While we did not explicitly reconstruct cross-feeding interactions, the lower prevalence of complete catabolic pathways for polysaccharides (relative to those for their mono- and oligomeric building blocks) suggests that many *Bifidobacterium* strains may depend on syntrophic relationships, both within the genus and with keystone degraders such as *Bacteroides* and *Segatella* (formerly *Prevotella*)[79–81]. Recent evidence for widespread HMO-degrading capacity across gut microbes[82] further supports the potential for cross-feeding involving bifidobacteria and other community members.

The genomic dataset analyzed in this study is skewed towards samples from high-income countries, highlighting the need for initiatives to expand collections of *Bifidobacterium* isolates and genomes from underrepresented populations in an ethical and culturally sensitive manner to capture global metabolic diversity[83]. Some observed within-species variability may reflect artifacts introduced by incomplete or contaminated MAGs and different assembly methods, underscoring the importance of expanding collections of high-quality MAGs and isolate genomes.

In summary, our study reveals how glycan foraging strategies vary across and within *Bifidobacterium* species, shaped by ecological factors, including host age, diet, and lifestyle. The comprehensive metabolic reconstruction and an automated pathway prediction pipeline provide a scalable framework for accurate functional annotation of bifidobacterial genomes and MAGs. This genomic compendium may inform the development of pro- and synbiotic formulations, including multi-strain consortia, whose members might efficiently colonize the gut across diverse lifestyle and dietary contexts.

Acknowledgments

We thank Robert Olson (Hack Biology LLC) for helping with mcSEED maintenance, Kang Liu (SBP Medical Discovery Institute Genomics Core) for library preparation and sequencing, Swetha Nakshatri (Washington University) and Kennedy Spann (UC San Diego) for technical assistance, Glycom A/S and DSM for generously providing individual HMOs, Dr. Takane Katayama (Kyoto University) for generously sharing *Bifidobacterium scardovii* JCM 12489 and insightful discussions. We are grateful to Dr. Mark Manary (Washington University) and study personnel at the Malawi College of Medicine for the provision of fecal samples used to isolate the Malawian bifidobacterial strains described in this report. Bangladeshi isolates were provided through a long-standing collaborative research program between Washington University and members of the International Center for Diarrheal Disease Research, Bangladesh (icddr,b) led by Dr. Tahmeed Ahmed. An MTA was established to transfer these strains to SBP Medical Discovery Institute. This work was supported by grants from the National Institutes of Health (NIH) (DK30292 to A.L.O. and J.I.G.) and the Bill & Melinda Gates Foundation (INV-016367). L.B. is the UC San Diego Chair of Collaborative Human Milk Research, endowed by the Family Larsson-Rosenquist Foundation, Switzerland.

Author contributions statement

A.A.A., D.A.R., M.J.B., J.I.G., and A.L.O. designed the study. A.A.A. did data curation and metabolic reconstruction. A.A.A., D.A.R., M.D.K., S.A.L., and A.L.O. developed the pathway prediction pipeline. J.L.G. isolated bacterial strains. M.C.H., J.E.K., and M.L.E. sequenced and assembled bacterial genomes. A.A.A. did growth and RNA-seq experiments. K.S., A.F., and L.B. isolated HMOs and did glycoprofiling analysis. A.A.A. wrote the initial draft with input from J.E.K. A.A.A., D.A.R., M.C.H., L.B., M.J.B., J.I.G., and A.L.O. edited the manuscript with invaluable assistance from co-authors.

Competing interests statement

D.A.R. and A.L.O. are co-founders of Phenobiome Inc., a company pursuing the development of personalized nutritional solutions to balance the gut microbiome. L.B. is a coinventor on patent applications related to the use of HMOs in preventing necrotizing enterocolitis and other inflammatory diseases. The remaining authors of this paper declare no competing interests.

Main text figures

Fig. 1. ***In silico* reconstruction of carbohydrate metabolism in bifidobacteria. a,** Overview of the computational framework. We analyzed the distribution of 589 metabolic functional roles (glycan transporters, CAZymes, downstream catabolic enzymes, transcription factors) across 263 reference *Bifidobacterium* genomes. Manual reconstruction of 68 carbohydrate utilization pathways enabled the assignment of binary pathway variants corresponding to predicted glycan utilization phenotypes based on specific genomic signatures (see **Extended Data Fig. 2**). This curated dataset was used to train an automated pathway prediction pipeline (glycobif), which outputs: (i) the distribution of functional roles across additional 2,820 *Bifidobacterium* genomes and (ii) a Binary Phenotype Matrix (BPM) reflecting the inferred presence or absence of pathways in each genome. Predicted phenotypes for 20 reference and 10 additional strains were compared with *in vitro* growth profiles to evaluate prediction accuracy. **b,** Comparison of functional gene annotations obtained via manual curation versus automated tools in the 263 reference *Bifidobacterium* genomes. Stacked bar plots show the distribution of 39,589 manually curated annotations across four categories: *new* = annotations that update non-specific predictions (e.g., hypothetical protein); *corrected* = annotations that replace specific but incorrect predictions; *refined* = annotations that add functional precision (e.g., substrate and linkage specificity for GHs); *same* = annotations that are essentially identical to automated output (**Supplementary Table 13**). **c**, Percentage of catabolic CAZymes (glycoside hydrolases, carbohydrate esterases, polysaccharide lyases) captured in the reconstructed metabolic pathways across the 263 reference *Bifidobacterium* genomes. Each point represents a genome

Fig. 2. Representation of carbohydrate utilization pathways across 3,083 *Bifidobacterium* genomes. **a,** Non-metric multidimensional scaling (NMDS) of a Hamming distance matrix derived from the presence/absence patterns of 68 predicted carbohydrate utilization pathways across 627 isolate genomes plus 2,456 metagenome assembled genomes (MAGs). Points represent genomes; spider lines connect genomes to their group (taxon) centroid. Colors and shapes of centroids indicate taxonomic groups. **b**, Predicted phenotypic richness (the total number of carbohydrate utilization pathways) at species and strain levels. Each point represents a genome. Box plots show the median (center line), interquartile range (IQR; box bounds), and full data range excluding outliers (whiskers, defined as 1.5× IQR). Statistical comparisons were

performed using a two-sided generalized linear model (GLM) with a Poisson distribution, followed by post hoc pairwise comparisons with Bonferroni correction. Sample size (n) per group corresponds to the number of genomes analyzed. **c,** Heatmap of the proportion of genomes within each taxon encoding the 68 predicted carbohydrate utilization pathways. Color intensity indicates the percentage of genomes that encode each pathway. Annotation rows at the bottom indicate pathway/phenotype classifications. Full names are provided in **Supplementary Table 5**.

Fig. 3. **Integrated genomic and transcriptomic analysis of xyloglucan metabolism in *Bc. kashiwanohense* Bg42221_1E1**. **a**, Gene clusters potentially driving xyloglucan degradation (phenotype XGL) in *Bc. kashiwanohense* Bg42221_1E1. **b,** Reconstructed xyloglucan degradation pathway in *Bc. kashiwanohense* Bg42221_1E1: (i) xyloglucan chains are potentially cleaved by extracellular endo-β-1,4-glucanase Xgl5A, (ii) released oligosaccharides are imported and metabolized inside the cell by a coordinated action of CAZymes and downstream catabolic enzymes. **c,** Predicted DNA-binding motif of the XglT transcriptional regulator potentially controlling xyloglucan metabolism genes. **d,** Growth curves of *Bifidobacterium* strains in MRS-AC supplemented with 0.5% tamarind xyloglucan. Data represent the mean ± s.d. of three biological replicates. **e,** Volcano plot showing differential gene expression ($\log_2$ fold change vs. $-\log_{10}$ adjusted P-value) in *Bc. kashiwanohense* Bg42221_1E1 grown in MRS-AC with tamarind xyloglucan (XGL) versus MRS-AC with lactose (Lac). Differential expression was assessed using moderated two-sided t-tests with empirical Bayes variance moderation. P-values were adjusted for multiple comparisons using the Benjamini–Hochberg procedure. Genes were considered differentially expressed at Padj < 0.01 and $|\log_2 FC| > 2$. Genes belonging to the reconstructed XglT, XylR, and XosR regulons, as well as *xyn* cluster genes, are highlighted. Exact log□FC values, test statistics, and adjusted P-values are provided in **Supplementary Table 21a**.

Fig. 4. **Comparative genomic and functional profiling of human milk oligosaccharide (HMO) utilization capabilities in *Bifidobacterium* strains**. **a**, Schematic representation of HMO utilization genes in selected Bangladeshi *Bifidobacterium* strains and their homology to H1 cluster genes from *Bl. infantis* ATCC 15697. **b,** Growth curves of *Bifidobacterium* strains in MRS-AC supplemented with pooled HMOs. Data represent the mean ± s.d. of three biological

replicates. Curves are color-coded based on the presence of specific HMO utilization gene clusters in the respective strains. **c,** HPLC-based quantification of HMO depletion from culture supernatants after 24 h. Data represent the percentage of utilized HMOs (mean of three biological replicates) relative to the medium control. Total HMO = total HMO utilized; total FHMO = total fucosylated HMO utilized; total SHMO = total sialylated HMO utilized. Concentrations of individual HMOs (nmol/mL) are provided in **Supplementary Table 18b**. **d**, Principal Component Analysis (PCA) based on combined growth metrics (maximum OD_{600}, area under the curve, and maximum growth rate) and percent utilization of individual HMOs. Each point represents a strain, color-coded by the presence of specific HMO utilization gene clusters. **e,** Volcano plot showing differential gene expression ($\log_2$ fold change vs. $-\log_{10}$ adjusted P-value) in *Bc. kashiwanohense* Bg42221_1E1 grown in MRS-AC with lacto-*N*-tetraose (LNT) versus MRS-AC with lactose (Lac). Differential expression was assessed using moderated two-sided t-tests with empirical Bayes variance moderation. P-values were adjusted for multiple comparisons using the Benjamini–Hochberg procedure. Genes were considered differentially expressed at Padj < 0.01 and $|\log_2 FC| > 2$. Genes belonging to the reconstructed NagR regulon are highlighted. Exact log□FC values, test statistics, and adjusted P-values are provided in **Supplementary Table 21b**.

Fig. 5. **Comparison of predicted carbohydrate utilization phenotypes with *in vitro* growth data**. **a**, Summary of *in vitro* growth profiles of 30 *Bifidobacterium* strains on 43 substrates. Growth, weak growth, and no growth were categorized based on strain-specific OD_{600} thresholds (*Methods*). The row annotation shows the geographical origin of each strain. The details about substrates are given in **Supplementary Table 15**; all growth curves are shown in **Supplementary Fig. 4**; raw OD_{600} data are provided in **Supplementary Table 16**. **b**, Comparison of 38 predicted carbohydrate utilization phenotypes with corresponding *in vitro* growth profiles for the same 30 strains. Predicted phenotypes were tested using a singular substrate, except IMO (panose and isomaltotriose), BglOS (cellobiose, gentiobiose, laminaritriose, and sophorose), and SHMO (3'-sialyllactose, 6'-sialyllactose). Prediction outcomes are color-coded to indicate agreement between predicted and observed phenotypes. The row annotation indicates whether genomes belong to the reference or extended dataset. The column annotation shows phenotype classification (glycan type). Summary data are provided in

Supplementary Table 17f; full names of abbreviations are provided in **Supplementary Table 5**.

References

1. Alessandri, G., van Sinderen, D. & Ventura, M. The genus bifidobacterium: From genomics to functionality of an important component of the mammalian gut microbiota running title: Bifidobacterial adaptation to and interaction with the host. *Comput Struct Biotechnol J* **19**, 1472–1487 (2021).
2. Arboleya, S., Watkins, C., Stanton, C. & Ross, R. P. Gut Bifidobacteria Populations in Human Health and Aging. *Front Microbiol* **7**, 1204 (2016).
3. Stewart, C. J. *et al.* Temporal development of the gut microbiome in early childhood from the TEDDY study. *Nature* **562**, 583–588 (2018).
4. Sakanaka, M. *et al.* Evolutionary adaptation in fucosyllactose uptake systems supports bifidobacteria-infant symbiosis. *Sci Adv* **5**, eaaw7696 (2019).
5. Arzamasov, A. A. & Osterman, A. L. Milk glycan metabolism by intestinal bifidobacteria: insights from comparative genomics. *Crit Rev Biochem Mol Biol* 1–23 (2023) doi:10.1080/10409238.2023.2182272.
6. Kujawska, M. *et al.* Succession of Bifidobacterium longum Strains in Response to a Changing Early Life Nutritional Environment Reveals Dietary Substrate Adaptations. *iScience* **23**, 101368 (2020).
7. Vatanen, T. *et al.* A distinct clade of Bifidobacterium longum in the gut of Bangladeshi children thrives during weaning. *Cell* (2022) doi:10.1016/j.cell.2022.10.011.
8. Orihara, K. *et al.* Characterization of Bifidobacterium kashiwanohense that utilizes both milk- and plant-derived oligosaccharides. *Gut Microbes* **15**, 2207455 (2023).
9. Taft, D. H. *et al.* Bifidobacterium Species Colonization in Infancy: A Global Cross-Sectional Comparison by Population History of Breastfeeding. *Nutrients* **14**, 1423 (2022).
10. Olm, M. R. *et al.* Robust variation in infant gut microbiome assembly across a spectrum of lifestyles. *Science* **376**, 1220–1223 (2022).
11. Derrien, M. *et al.* Gut microbiome function and composition in infants from rural Kenya and association with human milk oligosaccharides. *Gut Microbes* **15**, 2178793 (2023).
12. Tannock, G. W. *et al.* Comparison of the compositions of the stool microbiotas of infants fed goat milk formula, cow milk-based formula, or breast milk. *Appl. Environ. Microbiol.* **79**, 3040–3048 (2013).
13. Casaburi, G. *et al.* Metagenomic insights of the infant microbiome community structure and function across multiple sites in the United States. *Sci Rep* **11**, 1472 (2021).
14. Fukuda, S. *et al.* Bifidobacteria can protect from enteropathogenic infection through production of acetate. *Nature* **469**, 543–547 (2011).
15. Hirano, R. *et al.* Next-generation prebiotic promotes selective growth of bifidobacteria, suppressing Clostridioides difficile. *Gut Microbes* **13**, 1973835 (2021).
16. Belenguer, A. *et al.* Two routes of metabolic cross-feeding between Bifidobacterium adolescentis and butyrate-producing anaerobes from the human gut. *Appl. Environ. Microbiol.* **72**, 3593–3599 (2006).
17. Rios-Covian, D., Gueimonde, M., Duncan, S. H., Flint, H. J. & de los Reyes-Gavilan, C. G. Enhanced butyrate formation by cross-feeding between Faecalibacterium prausnitzii and Bifidobacterium adolescentis. *FEMS Microbiol. Lett.* **362**, (2015).
18. Laursen, M. F. *et al.* Bifidobacterium species associated with breastfeeding produce aromatic lactic acids in the infant gut. *Nat Microbiol* **6**, 1367–1382 (2021).

19. Shiver, A. L. *et al.* Genome-scale resources in the infant gut symbiont Bifidobacterium breve reveal genetic determinants of colonization and host-microbe interactions. *Cell* S0092-8674(25)00195–3 (2025) doi:10.1016/j.cell.2025.02.010.
20. Maldonado-Gómez, M. X. *et al.* Stable Engraftment of Bifidobacterium longum AH1206 in the Human Gut Depends on Individualized Features of the Resident Microbiome. *Cell Host Microbe* **20**, 515–526 (2016).
21. Frese, S. A. *et al.* Persistence of Supplemented Bifidobacterium longum subsp. infantis EVC001 in Breastfed Infants. *mSphere* **2**, e00501-17 (2017).
22. Beck, L. C. *et al.* Strain-specific impacts of probiotics are a significant driver of gut microbiome development in very preterm infants. *Nat Microbiol* **7**, 1525–1535 (2022).
23. Barratt, M. J. *et al.* Bifidobacterium infantis treatment promotes weight gain in Bangladeshi infants with severe acute malnutrition. *Sci Transl Med* **14**, eabk1107 (2022).
24. Button, J. E. *et al.* Dosing a synbiotic of human milk oligosaccharides and B. infantis leads to reversible engraftment in healthy adult microbiomes without antibiotics. *Cell Host Microbe* **30**, 712-725.e7 (2022).
25. Milani, C. *et al.* Bifidobacteria exhibit social behavior through carbohydrate resource sharing in the gut. *Sci Rep* **5**, 15782 (2015).
26. Albert, K., Rani, A. & Sela, D. A. Comparative Pangenomics of the Mammalian Gut Commensal Bifidobacterium longum. *Microorganisms* **8**, (2019).
27. Liu, J., Li, W., Yao, C., Yu, J. & Zhang, H. Comparative genomic analysis revealed genetic divergence between Bifidobacterium catenulatum subspecies present in infant versus adult guts. *BMC Microbiol* **22**, 158 (2022).
28. Arboleya, S. *et al.* Gene-trait matching across the Bifidobacterium longum pan-genome reveals considerable diversity in carbohydrate catabolism among human infant strains. *BMC Genomics* **19**, 33 (2018).
29. Bottacini, F. *et al.* Comparative genomics and genotype-phenotype associations in Bifidobacterium breve. *Sci Rep* **8**, (2018).
30. Liu, S. *et al.* Gene-Phenotype Associations Involving Human-Residential Bifidobacteria (HRB) Reveal Significant Species- and Strain-Specificity in Carbohydrate Catabolism. *Microorganisms* **9**, 883 (2021).
31. Magnúsdóttir, S. *et al.* Generation of genome-scale metabolic reconstructions for 773 members of the human gut microbiota. *Nat Biotechnol* **35**, 81–89 (2017).
32. Devika, N. T. & Raman, K. Deciphering the metabolic capabilities of Bifidobacteria using genome-scale metabolic models. *Sci Rep* **9**, 18222 (2019).
33. Schöpping, M., Gaspar, P., Neves, A. R., Franzén, C. J. & Zeidan, A. A. Identifying the essential nutritional requirements of the probiotic bacteria Bifidobacterium animalis and Bifidobacterium longum through genome-scale modeling. *NPJ Syst Biol Appl* **7**, 47 (2021).
34. Casey, J. *et al.* Transporter annotations are holding up progress in metabolic modeling. *Front. Syst. Biol.* **4**, (2024).
35. Overbeek, R. *et al.* The subsystems approach to genome annotation and its use in the project to annotate 1000 genomes. *Nucleic Acids Research* **33**, 5691–5702 (2005).
36. Bottacini, F. *et al.* Comparative genomics of the Bifidobacterium breve taxon. *BMC Genomics* **15**, 170 (2014).
37. Raman, A. S. *et al.* A sparse covarying unit that describes healthy and impaired human gut microbiota development. *Science* **365**, (2019).

38. Gehrig, J. L. *et al.* Effects of microbiota-directed foods in gnotobiotic animals and undernourished children. *Science* **365**, (2019).
39. Smith, M. I. *et al.* Gut microbiomes of Malawian twin pairs discordant for kwashiorkor. *Science* **339**, 548–554 (2013).
40. Turroni, F. *et al.* Genome analysis of Bifidobacterium bifidum PRL2010 reveals metabolic pathways for host-derived glycan foraging. *Proc Natl Acad Sci U S A* **107**, 19514–19519 (2010).
41. Mattarelli, P., Bonaparte, C., Pot, B. & Biavati, B. Proposal to reclassify the three biotypes of Bifidobacterium longum as three subspecies: Bifidobacterium longum subsp. longum subsp. nov., Bifidobacterium longum subsp. infantis comb. nov. and Bifidobacterium longum subsp. suis comb. nov. *Int J Syst Evol Microbiol* **58**, 767–772 (2008).
42. Chaplin, A. V. *et al.* Intraspecies Genomic Diversity and Long-Term Persistence of Bifidobacterium longum. *PLoS One* **10**, (2015).
43. Modesto, M. *et al.* Bifidobacterium longum subsp. iuvenis subsp. nov., a novel subspecies isolated from the faeces of weaning infants. *Int J Syst Evol Microbiol* **73**, (2023).
44. O'Connell Motherway, M. *et al.* Characterization of ApuB, an extracellular type II amylopullulanase from Bifidobacterium breve UCC2003. *Appl. Environ. Microbiol.* **74**, 6271–6279 (2008).
45. Kashima, T. *et al.* Identification of difructose dianhydride I synthase/hydrolase from an oral bacterium establishes a novel glycoside hydrolase family. *J Biol Chem* **297**, 101324 (2021).
46. LoCascio, R. G., Desai, P., Sela, D. A., Weimer, B. & Mills, D. A. Broad conservation of milk utilization genes in Bifidobacterium longum subsp. infantis as revealed by comparative genomic hybridization. *Appl Environ Microbiol* **76**, 7373–7381 (2010).
47. Sakurama, H. *et al.* Lacto-N-biosidase encoded by a novel gene of Bifidobacterium longum subspecies longum shows unique substrate specificity and requires a designated chaperone for its active expression. *J. Biol. Chem.* **288**, 25194–25206 (2013).
48. Garrido, D. *et al.* A novel gene cluster allows preferential utilization of fucosylated milk oligosaccharides in Bifidobacterium longum subsp. longum SC596. *Sci Rep* **6**, (2016).
49. Ojima, M. N. *et al.* Priority effects shape the structure of infant-type Bifidobacterium communities on human milk oligosaccharides. *ISME J* (2022) doi:10.1038/s41396-022-01270-3.
50. Komeno, M. *et al.* Two α-L-arabinofuranosidases from Bifidobacterium longum subsp. longum are involved in arabinoxylan utilization. *Appl Microbiol Biotechnol* **106**, 1957–1965 (2022).
51. Friess, L. *et al.* Two extracellular α-arabinofuranosidases are required for cereal-derived arabinoxylan metabolism by Bifidobacterium longum subsp. longum. *Gut Microbes* **16**, 2353229 (2024).
52. Tm, G. *et al.* Characterization and three-dimensional structures of two distinct bacterial xyloglucanases from families GH5 and GH12. *The Journal of biological chemistry* **282**, (2007).
53. J, R. *et al.* Mechanisms involved in xyloglucan catabolism by the cellulosome-producing bacterium Ruminiclostridium cellulolyticum. *Scientific reports* **6**, (2016).
54. Garrido, D., Kim, J. H., German, J. B., Raybould, H. E. & Mills, D. A. Oligosaccharide Binding Proteins from Bifidobacterium longum subsp. infantis Reveal a Preference for Host Glycans. *PLoS One* **6**, (2011).

55. Sela, D. A. *et al.* An infant-associated bacterial commensal utilizes breast milk sialyloligosaccharides. *J. Biol. Chem.* **286**, 11909–11918 (2011).
56. Sela, D. A. *et al.* Bifidobacterium longum subsp. infantis ATCC 15697 α-Fucosidases Are Active on Fucosylated Human Milk Oligosaccharides. *Appl Environ Microbiol* **78**, 795–803 (2012).
57. Garrido, D., Ruiz-Moyano, S. & Mills, D. A. Release and utilization of N-acetyl-d-glucosamine from human milk oligosaccharides by Bifidobacterium longum subsp. infantis. *Anaerobe* **18**, 430–435 (2012).
58. Arzamasov, A. A. *et al.* Human Milk Oligosaccharide Utilization in Intestinal Bifidobacteria Is Governed by Global Transcriptional Regulator NagR. *mSystems* e0034322 (2022) doi:10.1128/msystems.00343-22.
59. Egan, M., O'Connell Motherway, M., Ventura, M. & van Sinderen, D. Metabolism of Sialic Acid by Bifidobacterium breve UCC2003. *Appl Environ Microbiol* **80**, 4414–4426 (2014).
60. Egan, M. *et al.* Cross-feeding by Bifidobacterium breve UCC2003 during co-cultivation with Bifidobacterium bifidum PRL2010 in a mucin-based medium. *BMC Microbiol* **14**, (2014).
61. Pasolli, E. *et al.* Extensive Unexplored Human Microbiome Diversity Revealed by Over 150,000 Genomes from Metagenomes Spanning Age, Geography, and Lifestyle. *Cell* **176**, 649-662.e20 (2019).
62. Khoroshkin, M. S., Leyn, S. A., Van Sinderen, D. & Rodionov, D. A. Transcriptional Regulation of Carbohydrate Utilization Pathways in the Bifidobacterium Genus. *Front Microbiol* **7**, (2016).
63. Milani, C. *et al.* Genomic encyclopedia of type strains of the genus Bifidobacterium. *Appl Environ Microbiol* **80**, 6290–6302 (2014).
64. Odamaki, T. *et al.* Comparative Genomics Revealed Genetic Diversity and Species/Strain-Level Differences in Carbohydrate Metabolism of Three Probiotic Bifidobacterial Species. *Int J Genomics* **2015**, 567809 (2015).
65. Crociani, F., Alessandrini, A., Mucci, M. M. & Biavati, B. Degradation of complex carbohydrates by Bifidobacterium spp. *Int J Food Microbiol* **24**, 199–210 (1994).
66. Forster, S. C. *et al.* A human gut bacterial genome and culture collection for improved metagenomic analyses. *Nat Biotechnol* **37**, 186–192 (2019).
67. Poyet, M. *et al.* A library of human gut bacterial isolates paired with longitudinal multiomics data enables mechanistic microbiome research. *Nat Med* **25**, 1442–1452 (2019).
68. Lin, X. *et al.* The genomic landscape of reference genomes of cultivated human gut bacteria. *Nat Commun* **14**, 1663 (2023).
69. Hitch, T. C. A. *et al.* HiBC: a publicly available collection of bacterial strains isolated from the human gut. *Nat Commun* **16**, 4203 (2025).
70. Almeida, A. *et al.* A unified catalog of 204,938 reference genomes from the human gut microbiome. *Nat Biotechnol* **39**, 105–114 (2021).
71. Kim, C. Y. *et al.* Human reference gut microbiome catalog including newly assembled genomes from under-represented Asian metagenomes. *Genome Med* **13**, 134 (2021).
72. Zeng, S. *et al.* A compendium of 32,277 metagenome-assembled genomes and over 80 million genes from the early-life human gut microbiome. *Nat Commun* **13**, 5139 (2022).
73. Gounot, J.-S. *et al.* Genome-centric analysis of short and long read metagenomes reveals uncharacterized microbiome diversity in Southeast Asians. *Nat Commun* **13**, 6044 (2022).
74. Jin, H. *et al.* A high-quality genome compendium of the human gut microbiome of Inner Mongolians. *Nat Microbiol* **8**, 150–161 (2023).

75. Kim, M. *et al.* Higher pathogen load in children from Mozambique vs. USA revealed by comparative fecal microbiome profiling. *ISME Commun* **2**, 74 (2022).
76. de Crécy-Lagard, V. *et al.* A roadmap for the functional annotation of protein families: a community perspective. *Database (Oxford)* **2022**, baac062 (2022).
77. Price, M. N. & Arkin, A. P. Interactive tools for functional annotation of bacterial genomes. *Database* **2024**, baae089 (2024).
78. Zhu, L. *et al.* Captive Common Marmosets (Callithrix jacchus) Are Colonized throughout Their Lives by a Community of Bifidobacterium Species with Species-Specific Genomic Content That Can Support Adaptation to Distinct Metabolic Niches. *mBio* e0115321 (2021) doi:10.1128/mBio.01153-21.
79. Chang, H.-W. *et al.* Prevotella copri and microbiota members mediate the beneficial effects of a therapeutic food for malnutrition. *Nat Microbiol* **9**, 922–937 (2024).
80. Munoz, J., James, K., Bottacini, F. & Van Sinderen, D. Biochemical analysis of cross-feeding behaviour between two common gut commensals when cultivated on plant-derived arabinogalactan. *Microb Biotechnol* (2020) doi:10.1111/1751-7915.13577.
81. Fernandez-Julia, P., Black, G. W., Cheung, W., Van Sinderen, D. & Munoz-Munoz, J. Fungal β-glucan-facilitated cross-feeding activities between Bacteroides and Bifidobacterium species. *Commun Biol* **6**, 576 (2023).
82. Renwick, S. *et al.* Modulating the developing gut microbiota with 2'-fucosyllactose and pooled human milk oligosaccharides. *Microbiome* **13**, 44 (2025).
83. Browne, H. P. *et al.* Boosting microbiome science worldwide could save millions of children's lives. *Nature* **625**, 237–240 (2024).
84. Davis, J. J. *et al.* The PATRIC Bioinformatics Resource Center: expanding data and analysis capabilities. *Nucleic Acids Res* **48**, D606–D612 (2020).
85. Markowitz, V. M. *et al.* IMG: the Integrated Microbial Genomes database and comparative analysis system. *Nucleic Acids Res* **40**, D115-122 (2012).
86. Parks, D. H., Imelfort, M., Skennerton, C. T., Hugenholtz, P. & Tyson, G. W. CheckM: assessing the quality of microbial genomes recovered from isolates, single cells, and metagenomes. *Genome Res* **25**, 1043–1055 (2015).
87. Olm, M. R., Brown, C. T., Brooks, B. & Banfield, J. F. dRep: a tool for fast and accurate genomic comparisons that enables improved genome recovery from metagenomes through de-replication. *ISME J* **11**, 2864–2868 (2017).
88. Parks, D. H. *et al.* GTDB: an ongoing census of bacterial and archaeal diversity through a phylogenetically consistent, rank normalized and complete genome-based taxonomy. *Nucleic Acids Res* **50**, D785–D794 (2022).
89. Tonkin-Hill, G. *et al.* Producing polished prokaryotic pangenomes with the Panaroo pipeline. *Genome Biol* **21**, 180 (2020).
90. Katoh, K. & Standley, D. M. MAFFT Multiple Sequence Alignment Software Version 7: Improvements in Performance and Usability. *Mol Biol Evol* **30**, 772–780 (2013).
91. Minh, B. Q. *et al.* IQ-TREE 2: New Models and Efficient Methods for Phylogenetic Inference in the Genomic Era. *Mol. Biol. Evol.* **37**, 1530–1534 (2020).
92. Letunic, I. & Bork, P. Interactive Tree Of Life (iTOL) v5: an online tool for phylogenetic tree display and annotation. *Nucleic Acids Research* **49**, W293–W296 (2021).
93. Pritchard, L., Glover, R. H., Humphris, S., Elphinstone, J. G. & Toth, I. K. Genomics and taxonomy in diagnostics for food security: soft-rotting enterobacterial plant pathogens. *Anal. Methods* **8**, 12–24 (2015).

94. Seemann, T. Prokka: rapid prokaryotic genome annotation. *Bioinformatics* **30**, 2068–2069 (2014).
95. Overbeek, R. *et al.* The SEED and the Rapid Annotation of microbial genomes using Subsystems Technology (RAST). *Nucleic Acids Res.* **42**, D206-214 (2014).
96. Cantalapiedra, C. P., Hernández-Plaza, A., Letunic, I., Bork, P. & Huerta-Cepas, J. eggNOG-mapper v2: Functional Annotation, Orthology Assignments, and Domain Prediction at the Metagenomic Scale. *Mol Biol Evol* **38**, 5825–5829 (2021).
97. Zheng, J. *et al.* dbCAN3: automated carbohydrate-active enzyme and substrate annotation. *Nucleic Acids Res* gkad328 (2023) doi:10.1093/nar/gkad328.
98. Saier, M. H. *et al.* The Transporter Classification Database (TCDB): 2021 update. *Nucleic Acids Res* **49**, D461–D467 (2021).
99. Drula, E. *et al.* The carbohydrate-active enzyme database: functions and literature. *Nucleic Acids Res* **50**, D571–D577 (2022).
100. Kanehisa, M., Sato, Y., Kawashima, M., Furumichi, M. & Tanabe, M. KEGG as a reference resource for gene and protein annotation. *Nucleic Acids Res.* **44**, D457-462 (2016).
101. Novichkov, P. S. *et al.* RegPrecise: a database of curated genomic inferences of transcriptional regulatory interactions in prokaryotes. *Nucleic Acids Res* **38**, D111–D118 (2010).
102. Steinegger, M. & Söding, J. MMseqs2 enables sensitive protein sequence searching for the analysis of massive data sets. *Nat Biotechnol* **35**, 1026–1028 (2017).
103. Buchfink, B., Xie, C. & Huson, D. H. Fast and sensitive protein alignment using DIAMOND. *Nat. Methods* **12**, 59–60 (2015).
104. Abraham, A. *et al.* Machine learning for neuroimaging with scikit-learn. *Front Neuroinform* **8**, 14 (2014).
105. Kuhn, M. Building Predictive Models in R Using the caret Package. *Journal of Statistical Software* **028**, (2008).
106. Hibberd, M. C. *et al.* Bioactive glycans in a microbiome-directed food for children with malnutrition. *Nature* **625**, 157–165 (2024).
107. Oksanen, J. *et al.* vegan: Community Ecology Package. (2022).
108. Lenth, R. V. *et al.* emmeans: Estimated Marginal Means, aka Least-Squares Means. (2022).
109. Wickham, Hadley. *Ggplot2: Elegant Graphics for Data Analysis*. (Springer-Verlag, New York, 2016).
110. Gu, Z., Eils, R. & Schlesner, M. Complex heatmaps reveal patterns and correlations in multidimensional genomic data. *Bioinformatics* **32**, 2847–2849 (2016).
111. Gilchrist, C. L. M. & Chooi, Y.-H. clinker & clustermap.js: automatic generation of gene cluster comparison figures. *Bioinformatics* **37**, 2473–2475 (2021).
112. Berger, P. K. *et al.* Stability of Human-Milk Oligosaccharide Concentrations Over 1 Week of Lactation and Over 6 Hours Following a Standard Meal. *J Nutr* **152**, 2727–2733 (2023).

METHODS

Collection of *Bifidobacterium* genomes

Reference genomes for the manual *in silico* metabolic reconstruction were retrieved from Bacterial and Viral Bioinformatics Resource Center (BV-BRC)[84] and Integrated Microbial Genomes (IMG)[85] databases as of October 2020. We selected 335 genomes based on the following criteria: (i) human or probiotic product-derived *Bifidobacterium spp.* isolates, (ii) number of contigs ≤ 200, (iii) CheckM[86] completeness ≥ 97 % and contamination ≤ 3%. Additionally, we sequenced 31 genomes of cultured isolates from fecal samples obtained from Bangladeshi children[37,38]. The resulting reference set of 366 genomes was clustered using dRep (v3.4.2)[87] at a 99.95% ANI threshold ("dRep dereplicate -pa 0.9 -sa 0.9995 -nc 0.35 --S_algorithm ANImf"), yielding 263 non-redundant genomes (**Supplementary Table 2**).

Additional human gut-derived *Bifidobacterium* genomes were collected from prior studies. These included isolate genomes from HBC[66], BIO-ML[67], and CGR[68] collections, and MAGs from UHGG[70], KIJ[71], ELGG[72], SPMP[73], and IMGG[74] collections and other datasets[75]. We used the same selection criteria for both isolate genomes and MAGs: (i) *Bifidobacterium* spp. based on Genome Taxonomy Database (GTDB) taxonomy[88] excluding *Bifidobacterium leopoldii* and *Bifidobacterium vaginale*, (ii) number of contigs ≤ 200, (iii) CheckM completeness ≥ 97% and contamination ≤ 3%. The resulting 4,944 genomes were clustered via dRep using the following command "dRep dereplicate -pa 0.9 -sa 0.999 -nc 0.35 --S_algorithm fastANI", yielding 2811 non-redundant genomes (**Supplementary Table 3**). We also sequenced nine genomes of strains isolated from Bangladeshi and Malawian infants previously[37–39], resulting in 2,820 additional genomes.

Isolation and sequencing of *Bifidobacterium* strains from Bangladeshi and Malawian donors

Fecal samples used for culturing Bangladeshi bifidobacterial strains were collected during studies conducted by the International Centre for Diarrhoeal Disease Research (icddr,b). These were (i) the MAL-ED birth cohort study of children aged 0-24 months (Interactions of Enteric Infections and Malnutrition and the Consequences for Child Health and Development; ClinicalTrials.gov identifier NCT02441426) and (ii) a cohort of healthy 12-24 month-old Bangladeshi children enrolled in parallel with children with acute malnutrition in a study of

microbiota-directed complementary food (MDCF) prototypes (ClinicalTrials.gov identifier NCT03084731)[37,38]. Both studies were approved by the Ethical Review Committee of the icddr,b. Bifidobacterial strains were also isolated from fecal samples collected in a previously reported study of Malawian twins discordant for acute malnutrition[39]. The protocol was approved by the College of Medicine Research Ethics Committee of the University of Malawi and by the Human Research Protection Office of Washington University in St. Louis. Written informed consent, including provisions for future use of materials, was provided by the parents or guardians of participating children before enrolment. The details of genome sequencing and assembly are provided in *Supplementary Methods*.

Taxonomy inference

Initial taxonomic assignments for the 263 reference *Bifidobacterium* genomes were retrieved from NCBI and BV-BRC for public genomes or inferred from 16S rRNA gene sequencing for Bangladeshi isolates. To refine these assignments, we built a pangenome via Panaroo (v1.3.2)[89]. Concatenated nucleotide sequences of 487 identified core genes (**Supplementary Table 12**) were aligned using MAFFT (v7.515)[90]. A maximum-likelihood phylogenetic tree was built in IQ-TREE (v2.2.0.3)[91] and visualized via iTOL (v5)[92]. Pairwise ANI values (ANIb) were calculated using pyani (v0.2.12)[93]. The exact commands and parameters are provided in **Supplementary Code File 1**. The resulting tree topology was manually inspected to verify and correct taxonomic assignments of genomes based on their co-clustering with branches corresponding to the type or well-characterized strains of *Bifidobacterium* species and subspecies. ANI matrices were used to delineate the within-species structure for *Bifidobacterium longum* and *Bifidobacterium catenulatum* species. GTDB-based taxonomies of 2,820 additional genomes were retrieved from original publications and refined via ANI comparisons with 263 reference genomes. Species assignments were made if ANI to the closest reference genome was > 95%, and subspecies assignments if > 97%.

Gene prediction and functional annotation

Protein-coding sequences were predicted and annotated with Prokka (v1.14.6)[94] using default settings. The 263 reference genomes were additionally annotated via RASTtk (v1.073)[95] and EggNOG-mapper (v2.1.12)[96] with default settings (**Supplementary Table 13**). The

representation of CAZymes in 263 genomes was analyzed using dbCAN (v4.0.0)[97]. HMMER, dbCAN-sub, and DIAMOND-based searches against the CAZy database were used for CAZyme identification. Only GHs, CEs, and polysaccharide lyases predicted by two or more methods were retained.

Subsystems-based annotation and *in silico* metabolic reconstruction of glycan utilization pathways

We used a subsystems-based approach implemented in the SEED platform[35,95] to reconstruct carbohydrate utilization pathways encoded in reference 263 *Bifidobacterium* strains. RASTtk-annotated genomes were uploaded to mcSEED (microbial community SEED), a clone of the SEED annotation environment. We created 25 subsystems that captured the representation of genes that implement *functional roles* (glycan transporters, CAZymes, downstream catabolic enzymes, and transcriptional regulators) involved in carbohydrate utilization (**Supplementary Table 4**). The list of functional roles was compiled via extensive literature search and using the information from Transporter Classification (TCDB)[98], Carbohydrate Active Enzyme (CAZy)[99], Kyoto Encyclopedia of Genes (KEGG)[100], and RegPrecise[101] databases. This knowledge was used to manually curate the automated functional annotations of protein-coding genes in a subset of reference *Bifidobacterium* genomes (e.g., type strains) where the respective functional roles had been experimentally characterized. Additional functional gene annotation to fill gaps in metabolic pathways was based on three genome context techniques: (i) clustering of genes on the chromosome (operons), (ii) co-regulation of genes by a common transcription factor, and (iii) co-occurrence of genes across related genomes. The approach used to reconstruct the regulons of transcription factors potentially regulating carbohydrate metabolism is outlined in *Supplementary methods*.

The propagation of curated annotations (corresponding to 589 functional roles) across all 263 reference genomes was performed using homology-based methods implemented in mcSEED. Orthologs were detected automatically using predefined protein family classifications such as PGFams (cross-genus protein families) and PLFams (genus-specific protein families)[84]. These assignments were manually refined by examining the gene neighborhood for each functional role. Genes with conserved gene neighborhoods were classified as orthologous, while

paralogs were assigned distinct functional annotations. Overall, 39,589 out of 541,418 protein-coding gene annotations in 263 reference *Bifidobacterium* genomes were curated.

Next, we reconstructed 72 catabolic pathways spanning 25 subsystems (**Supplementary Table 5**). Many pathways included alternative biochemical modules (routes) driven by different sets of catabolic enzymes and diverse glycan transporters. For each pathway, we defined genomic signatures — sets of genes encoding functional roles that together represent the minimal gene complement required to form a complete pathway for the utilization or degradation of a specific carbohydrate (**Supplementary Table 6**). *Utilization* was defined as a process when a glycan molecule (mono- or oligosaccharide) is transported into the cell and then catabolized using a combination of CAZymes and downstream catabolic enzymes. *Degradation* referred to the partial hydrolysis of a glycan (e.g., a polysaccharide) by extracellular CAZymes, with the resulting mono- and oligosaccharides subsequently transported into the cell and metabolized.

We used the presence or absence of genes matching each genomic signature to assign a detailed pathway variant to each genome: (i) transporter + catabolic pathway ("U"), (ii) catabolic pathway without transporter ("P"), (iii) no catabolic pathway ("N") (**Supplementary Tables 6,8**). For the purpose of automated phenotype profiling, these assignments were simplified into binary phenotypes: a complete pathway ("U") indicated predicted utilization or degradation and was assigned phenotype "1", while incomplete ("P") or missing ("N") pathway variants indicated no utilization and were assigned phenotype "0". The resulting set of 72 predicted carbohydrate utilization phenotypes across 263 strains comprised the reference Binary Phenotype Matrix (BPM) (**Supplementary Table 7**). Four pathways (GalNAc, ManAc, Man, and GalA), for which all strains in the reference set were assigned variants "P" or "N" and phenotype "0", respectively, were retained in the BPM but excluded from the pathway prediction pipeline.

Pathway prediction pipeline (glycobif)

The workflow used to predict the carbohydrate utilization pathways encoded in additional 2,820 *Bifidobacterium* genomes is schematically illustrated in **Fig. 1a**. We first constructed a reference database containing (i) 39,589 functionally annotated protein sequences from 25 curated mcSEED subsystems across 263 reference genomes, and (ii) an additional set of 52,990 outgroup proteins (not captured in the subsystems) clustered at 95% amino acid identity and 95% coverage using MMSeqs2 (v14.7e284)[102]. Proteins encoded in the 2,820 query genomes were annotated by

mapping their sequences to the reference database using DIAMOND (v2.1.4)[103]. To handle multidomain proteins, we first selected the top 50 hits for each query based on bitscore and clustered the alignment coordinates using DBSCAN (scikit-learn v1.2.1)[104]. Cluster centers were treated as potential domain boundaries, which were used to split query proteins into discrete domains, with database hits attributed to each individual domain. For each resulting domain with ≥ 35 amino acids, we applied the Gaussian kernel density modeling (*KernelDensity* function from *sklearn.neighbors*) to the distribution of sequence identity values, and used the highest local minimum (*argrelextrema* function from *sklearn.signal*) to filter out low-confidence hits. Annotations were assigned by majority vote from high-scoring, domain-specific reference hits. High-identity hits to outgroup proteins from the reference database were used as criteria to vote against applying annotation to a given query. This pipeline yielded 419,055 annotated protein sequences.

These annotations, together with the BPM for 263 reference genomes, were integrated into a machine learning-based pipeline to predict the presence ("1") or absence ("0") of carbohydrate utilization pathways in additional 2,820 genomes. We evaluated over 30 machine learning methods implemented in the *Caret* package (v6.0.86)[105] using a leave-one-out cross-validation approach: for each reference genome, a model was trained on the remaining 262 genomes and then used to predict the binary variant for the held-out genome. This process was repeated for every pathway. Random forest was identified as the best-performing model based on prediction accuracy. Pathway-specific random forest models were then trained using the full reference set, excluding four pathways (GalNAc, ManAc, Man, and GalA) for which all genomes had predicted binary phenotype "0". The list of functional roles used as model predictors for each remaining pathway was manually curated to match the genomic signatures delineating pathway variants (**Supplementary Table 6**). Model parameters were optimized using grid search, and mock genomes with custom genomic signatures were added to the training set to ensure that rare combinations from the reference collection were adequately learned and to improve model performance on incomplete MAGs. The resulting models were used to predict the presence or absence (1/0) of 68 carbohydrate utilization pathways in 2,820 genomes (**Supplementary Table 9**).

The representation of 29 additional metabolic pathways (e.g., the biosynthesis of B vitamins and amino acids) in both 263 reference and 2,820 additional genomes was inferred via a similar annotation pipeline as recently published[106] (**Supplementary Table 11**).

Visualization and statistical analysis

Non-metric multidimensional scaling (NMDS) was used for the ordination of the Hamming distance matrix calculated from the merged BPM of 3,083 genomes. PERMANOVA and a test for the homogeneity of multivariate dispersions were performed using the *adonis2* and *betadisper* functions in the *vegan* package (v2.6-8)[107]. Differences in predicted phenotypic richness were assessed via a generalized linear model (GLM) assuming Poisson distribution; post hoc comparisons with Bonferroni correction were conducted using the *emmeans* package (v1.10.6)[108]. Fisher's exact test was used for the enrichment analysis of pathway representation. For each of the 68 carbohydrate utilization pathways, 2×2 contingency tables were constructed. Rows denoted the absence/presence of predicted pathways ("0" or "1"), whereas columns represented metadata categories: age group (age < 3 years vs. age ≥ 3) or host lifestyle (Westernized vs. non-Westernized)[61]. P-values were corrected for multiple testing using the Benjamini-Hochberg procedure, with Padj ≤ 0.01 considered significant (**Supplementary Table 14**). Odds ratios were calculated using the *fisher.test* function. Principal component analysis (PCA) was used for the ordination of growth and HMO consumption data. Data visualization was performed using *ggplot2* (v3.5.1)[109], *ComplexHeatmap* (v2.18.0)[110], and clinker (v0.0.27)[111]. Code for all analyses is provided in **Supplementary Code File 1**.

***In vitro* growth of *Bifidobacterium* strains on selected carbohydrates**

All strains except *B. scardovii* JCM 12489 were routinely grown in dextrose-free Lactobacilli de Man, Rogosa & Sharpe broth (Alpha Biosciences) supplemented with 0.34% (wt/vol) sodium ascorbate, 0.029% (wt/vol) L-cysteine-HCl monohydrate, and 10 mg/mL lactose (MRS-AC-Lac) in a chamber maintained with a gas mix of 10% H_2, 10% CO_2, and 80% N_2 (Coy Laboratory Products). The MRS-C-Lac medium without sodium ascorbate was used for *B. scardovii* JCM 12489. The growth of 30 *Bifidobacterium* strains on 47 substrates (**Supplementary Table 15**) was measured using a custom carbohydrate array constructed in flat-bottom half-area 96-well plates (Costar). Wells were filled with 55 µl of a sterilized carbohydrate stock at 2×

concentration (10 to 20 mg/mL) and transferred to the chamber 48 h before the experiment. Each substrate was tested in triplicate (or duplicate in a few cases). Sterile water and lactose served as negative and positive controls.

Cultures for assay inoculations were grown overnight at 37 °C in MRS-AC-Lac, diluted 1:100 into fresh medium, and incubated for 8 h. Cultures were then adjusted to OD = 0.6, and 100 µL aliquots were harvested at 5,000 × g for 5 min and resuspended in 6 mL of 2× MRS-AC (2× MRS-C for *B. scardovii*) without added carbohydrate. Each well in the carbohydrate array was loaded with 55 µL of inoculated 2× medium to make individual 110 µL cultures. Growth was monitored by measuring OD_{600} every 15 or 30 minutes for 40 h under constant linear shaking using a Synergy H1 Plate Reader (BioTek Instruments). Raw OD_{600} data were exported using Gen5 software (v2.05.5) and analyzed in R (v4.3.2). For all strains except *B. pseudocatenulatum* M26A_2F1 growth on each glycan was classified as follows: (i) no growth ("−") if mean OD_{600} never exceeded 10% of the strain's highest OD_{600} within a panel of carbon sources, (ii) weak growth ("w") if mean OD_{600} did not exceed 25% of maximum OD_{600}, (iii) growth ("+") if mean OD_{600} was above 25% of maximum OD_{600} (**Supplementary Fig. 4**; **Supplementary Table 16**). For *B. pseudocatenulatum* M26A_2F1, thresholds were increased to 22% and 55%, respectively, due to some outgrowth in basal MRS-AC lacking an added substrate.

Comparison of predicted phenotypes with growth data

Predicted carbohydrate utilization phenotypes were compared with growth data from this work or prior literature[8,28,36]. A predicted binary phenotype "1" was classified as a true positive (TP) if it matched with growth phenotypes "+/w" and as a false positive (FP) if it matched with "−". A predicted binary phenotype "0" was considered a true negative (TN) if it matched with a growth phenotype "−" and a false negative (FN) if it matched with "+/w". Most predicted utilization phenotypes were tested using individual substrates. Exceptions included phenotypes IMO, for which the growth was tested on panose and isomaltotriose, BglOS (cellobiose, gentiobiose, laminaritriose, and sophorose), and SHMO (3'-sialyllactose, 6'-sialyllactose). For these cases, growth ("+/w") on at least one substrate was considered as a TP for a predicted binary phenotype "1", and the absence of growth on all tested substrates was considered a TN for "0". Standard

binary classification metrics were calculated from TP, TN, FP, and FN counts (**Supplementary Table 17**).

Glycoprofiling of HMO consumption

Overnight cultures of *Bifidobacterium* strains grown in MRS-AC-Lac were inoculated (0.5–1% [vol/vol]) into fresh medium and cultured to OD_{600}=0.6. Cells were harvested at 5,000 × g for 5 min, washed with sugar-free MRS-AC, and used to inoculate 200 µL of MRS-AC supplemented with an HMO mixture (10 mg/mL, isolated from pooled human milk from ≥ 25 different donors) in 96-well plates (Costar) at OD_{600}=0.005. Triplicate 100 µL samples of culture supernatant were collected at 8 or 24 h time points in separate experiments, filtered through Spin-X Centrifuge Tube Filter (0.22 µm, Costar), snap-frozen in liquid nitrogen, and stored at −80 °C. HMO concentrations in supernatants were analyzed by high-performance liquid chromatography (HPLC) with fluorescence detection[112]. Media samples (10 µL) were spiked with maltose as an internal standard, lyophilized, and labeled with the fluorophore 2-aminobenzamide (2AB). 2AB-labeled HMOs were separated on a TSKgel Amide-80 column (2.0 mm ID × 15 cm, 3 µm; Tosoh Bioscience) and detected at 360 nm excitation / 425 nm emission on Dionex Ultimate 3000 (Thermo Fisher Scientific). Nineteen HMO structures were annotated based on standard retention times and quantified relative to the internal standard: 2'-fucosyllactose (2'FL), 3-fucosyllactose (3FL), lactodifucotetraose (LDFT), 3'-sialyllactose (3'SL), 6'-sialyllactose (6'SL), lacto-*N*-tetraose (LNT), lacto-*N*-neotetraose (LNnT), lacto-*N*-fucopentaose (LNFP) I/II/III, sialyllacto-*N*-tetraose (LST) b and c, difucosyllacto-*N*-tetraose (DFLNT), lacto-*N*-hexaose (LNH), disialyllacto-*N*-tetraose (DSLNT), fucosyllacto-*N*-hexaose (FLNH), difucosyllacto-*N*-hexaose (DFLNH), fucodisialyllacto-*N*-hexaose (FDSLNH), disialyllacto-*N*-hexaose (DSLNH). Total HMO concentration was calculated as the sum of individual HMO concentrations (**Supplementary Table 18**). HMO utilization at 8 or 24 h was calculated relative to HMO concentrations in the medium controls.

Transcriptional profiling (RNA-seq)

An overnight culture of *Bc. kashiwanohense* Bg42221_1E1 grown in MRS-AC-Glc was harvested at 5,000 × g for 5 min, washed in sugar-free MRS-AC, and used to inoculate MRS-AC supplemented with either 10 mg/mL of glucose, lactose, lacto-*N*-tetraose, or 5 mg/mL of

tamarind xyloglucan at OD_{600}=0.01. Samples (2 mL, biological triplicates) were collected at the early exponential phase (OD_{600}=0.35) and pelleted in a prechilled centrifuge at 4,800 × g for 5 min. Cell pellets were snap-frozen in liquid nitrogen and stored at −80 °C until further use. The detailed RNA extraction protocol is described in *Supplementary methods*. Ribosomal RNA was depleted with the NEBNext rRNA depletion kit for bacteria (New England Biolabs) and a set of 20 pooled sequence-specific probes for *Bc. kashiwanohense* Bg42221_1E1 designed using the NEBNext Custom RNA Depletion Design Tool v1.0 (**Supplementary Table 20**). Barcoded libraries were made with the NEBNext Ultra II directional RNA library prep kit for Illumina (New England Biolabs). Libraries were pooled and sequenced (single-end 75-bp reads) on Illumina NextSeq 500 using the High Output V2 kit (Illumina). The details of sequencing data analysis are provided in *Supplementary methods*.

Data availability

Genomes of *Bifidobacterium* isolates sequenced in this study have been deposited in GenBank (https://www.ncbi.nlm.nih.gov/bioproject/PRJNA1126848). Nucleotide FASTA and annotated protein FASTA files of 263 reference genomes are available on Figshare (https://doi.org/10.6084/m9.figshare.26053936). Additional *Bifidobacterium* genomes and MAGs were retrieved from the following publicly available databases and datasets: BV-BRC (https://www.bv-brc.org), IMG (https://img.jgi.doe.gov), BIO-ML (https://www.ncbi.nlm.nih.gov/bioproject/PRJNA544527), CGR (https://www.ncbi.nlm.nih.gov/bioproject/PRJNA482748), CGR2 (https://www.ncbi.nlm.nih.gov/bioproject/PRJNA903559), UHGG (http://ftp.ebi.ac.uk/pub/databases/metagenomics/mgnify_genomes), KIJ (https://www.decodebiome.org/HRGM1), ELGG (https://zenodo.org/records/6969520), SPMP (https://figshare.com/collections/SPMP/5993596), IMGG (https://www.ncbi.nlm.nih.gov/bioproject/PRJNA763692). The RNA-seq data set has been deposited in Gene Expression Omnibus (https://www.ncbi.nlm.nih.gov/geo/query/acc.cgi?acc=GSE239955). Source data are provided on GitHub (https://github.com/Arzamasov/glycobif).

Code availability

Code detailing the data analysis steps is available on GitHub (https://github.com/Arzamasov/compendium_manuscript) and **Supplementary Code File 1.** The pipeline for analyzing the representation of carbohydrate utilization pathways encoded in bifidobacterial genomes (glycobif) is available on GitHub (https://github.com/Arzamasov/glycobif).

Supplementary information

Extended data figures

Extended Data Fig. 1. **Pairwise average nucleotide identity (ANI) analysis of reference *B. longum* and *B. catenulatum* genomes**. **a,** Pairwise ANI values for 28 *B. longum* genomes. For comparative purposes, this set contained 15 genomes from the reference collection (names are in bold) and 13 additional genomes, including the type strains of *Bl. suis* and *Bl. suillum* of non-human origin. Black lines indicate taxonomic groupings used in this study; blue lines denote the additional delineation proposed by Modesto et al.[43]. **b,** Pairwise ANI values for 11 reference *B. catenulatum*, *B. hominis*[69], and *B. pseudocatenulatum* genomes. Black lines indicate taxonomic groupings used in this study; NCBI and GTDB taxonomy assignments are shown in blue.

Extended Data Fig. 2. **Reconstruction of carbohydrate utilization pathways and associated phenotypes**. (1) A reference set of 263 *Bifidobacterium* genomes (**Supplementary Table 2**) and a list of 589 curated functional roles (**Supplementary Table 4**) were used to populate 25 metabolic subsystems capturing catabolic pathways for 68 glycans. (2) Functional gene annotation was performed using homology-based methods and three genome context techniques: (i) clustering of genes on the chromosome (operons), (ii) co-regulation of genes by a common transcription factor, and (iii) co-occurrence of genes across related genomes. Carbohydrate utilization pathways were reconstructed based on the distribution of functional roles. (3) Each genome was assigned a detailed pathway variant based on the presence of signature genes (**Supplementary Table 6**). These variants were then converted to predicted binary phenotypes (1 = utilizer, 0 = non-utilizer) to create a Binary Phenotype Matrix (BPM).

Extended Data Fig. 3. **Representation of predicted carbohydrate utilization pathways in *B. catenulatum* and *B. hominis* genomes**. The heatmap shows the hierarchical clustering of the Binary Phenotype Matrix (BPM) for 68 carbohydrate utilization pathways (columns) predicted in 110 *B. catenulatum* and 26 *B. hominis* genomes (rows). Pathway/phenotype classifications are shown in the bottom annotation tracks; taxonomic assignments are indicated on the right. Names of type strains are in bold. Full names pathway/phenotype names are provided in **Supplementary Table 5**.

Extended Data Fig. 4. **Genomics-based reconstruction of pathways involved in the utilization of monosaccharide derivatives**. **a,** Gene clusters potentially driving D-glucuronate (GlcA) utilization by *Bl. infantis* JG_Bg463 and glucuronide (GluA) utilization by *B. breve* Bg41721_1C11. Orthologous genes are linked, and the link color represents the sequence identity between corresponding protein products. **b,** Reconstructed D-glucuronate and glucuronide utilization pathways. **c**, Growth curves of selected *Bifidobacterium* strains in MRS-AC supplemented with 1% D-glucuronic acid. Data represent the mean ± s.d. of three biological replicates. **d**, Gene clusters potentially driving the utilization of (i) sugar alcohols D-mannitol (Mtl), D-sorbitol (Stl), and *myo*-inositol (Ino), (ii) sugar acids D-gluconate (Gco) and D-galactonate (Glt), (iii) L-ascorbate (Asc). **e,** Reconstructed utilization pathways for monosaccharide derivatives. **f,** Gene cluster (*nan*) driving sialic acid (Neu5Ac) utilization by *B. breve* strains. **g,** Neu5Ac utilization pathway in *B. breve*. **h**, Growth curves of selected *B. breve* strains in MRS-AC supplemented with 1% *N*-acetylneuraminic acid. Data represent the mean ± s.d. of three biological replicates.

Extended Data Fig. 5. **Representation of metabolic pathways in 28 selected *B. longum* isolate genomes**. For comparative purposes, this dataset includes 15 genomes from the reference collection (names in bold) and 13 additional genomes, primarily of non-human origin, including type strains of *Bl. suis* and *Bl. suillum*. Annotation rows at the bottom represent pathway/phenotype classifications. Annotation columns on the right denote taxonomic groupings: the left column reflects assignments used in this study; the right column showing subspecies delineation proposed by Modesto et al.[43]. **a,** Representation of 68 carbohydrate utilization pathways and associated metabolic phenotypes. Full names are provided in **Supplementary Table 5**. **b,** Representation of 29 additional pathways, including the biosynthesis of amino acids and B vitamins, and urea utilization.

Extended Data Fig. 6. Representation of core biosynthetic pathways across 3,083 *Bifidobacterium* genomes. The heatmap depicts the prevalence of metabolic pathways corresponding to: (i) B vitamin and amino acid biosynthesis, (ii) urea utilization (Urea_d) within each taxon. Color intensity indicates the proportion of genomes that encode the respective metabolic pathway.

Extended Data Fig. 7. **Genomics-based reconstruction of polysaccharide degradation and oligosaccharide utilization pathways**. **a**, Alignment of the amino acid sequences of xyloglucan endo-β-1,4-glucanases (xyloglucanases): PpXG5 from *Paenibacillus pabuli* XG5 (characterized), Xgl5A and Xgl5B from *Bc. kashiwanohense* Bg42221_1E1 (putative). Conserved catalytic amino acid residues are highlighted in bold red, and conserved glycan-binding residues are in bold. **b,** Gene clusters potentially driving the degradation of (arabino)xylan and the utilization of released oligosaccharides in *Bc. kashiwanohense* Bg42221_1E1. **c,** Predicted DNA-binding motifs of transcription factors potentially controlling the expression of the gene clusters in **b**. Motifs were built based on operator sequences in the RegPrecise database and identified in this work (**Supplementary Table 19**). **d**, Gene clusters potentially driving β-mannose oligosaccharide utilization (phenotype bMnOS) in *B. breve* Bg41721_1C11 and β-mannan degradation (phenotype bMAN) in *B. dentium* LFYP24. Orthologous genes are linked, and the link color represents the sequence identity between corresponding protein products. **e**, Reconstructed β-mannose oligosaccharide utilization and β-mannan degradation pathways. Names of previously characterized enzymes and transporters are in bold. **f**, Growth curves of selected *Bifidobacterium* strains in the medium supplemented with 0.5% mannotriose or 0.5% konjac glucomannan. Data represent the mean ± s.d. of three biological replicates. **g,** Predicted MnbR DNA-binding motif based on operator sequences identified in this work (**Supplementary Table 19**).

Extended Data Fig. 8. Pathway enrichment analysis across 3,083 *Bifidobacterium* genomes. Pathways significantly enriched in specific groups (Benjamini–Hochberg adjusted $P \leq 0.01$; two-sided Fisher's exact test) are shown. Points represent odds ratios, and horizontal lines indicate 95% confidence intervals. Pathways with infinite odds ratios are present exclusively in one group. Exact adjusted P-values are provided in **Supplementary Table 14**. **a**, Comparison between genomes from "Westernized (age < 3)" vs. "Westernized (age ≥ 3)" groups. **b**, Comparison between genomes from "non-Westernized (age < 3)" vs. "non-Westernized (age ≥ 3)" groups. **c**, Comparison between genomes from "Westernized (age < 3)" vs. "non-Westernized (age < 3)" groups. **d**, Comparison within individual taxa between genomes from "Westernized" vs. "non-Westernized" groups.

Extended Data Fig. 9. HPLC-based quantification of human milk oligosaccharide (HMO) depletion from culture supernatants after 8 h. Data represent the percentage of utilized HMOs (mean of three biological replicates) relative to the medium control. Total HMO = total HMO utilized; total FHMO = total fucosylated HMO utilized; total SHMO = total sialylated HMO utilized. Concentrations of individual HMOs (nmol/mL) are provided in **Supplementary Table 18a**.

Supplementary figures

Supplementary Fig. 1. **Phylogenetic tree of 263 reference *Bifidobacterium* genomes**. The maximum-likelihood tree was constructed from a concatenated alignment of nucleotide sequences of 487 core genes. Node bootstrap support values are indicated by color.

Supplementary Fig. 2. **Concordance between phylogeny and predicted phenotypes**. The tanglegram compares the phylogenetic tree of 263 reference *Bifidobacterium* genomes with the Hamming-distance dendrogram derived from the Binary Phenotype Matrix (BPM). Lines connecting matching genomes are colored by taxonomic assignment.

Supplementary Fig. 3. **Variability in predicted carbohydrate utilization phenotypes across 263 reference *Bifidobacterium* strains**. The heatmap shows the hierarchical clustering (Hamming distance and average linkage) of the Binary Phenotype Matrix (BPM) for 68 carbohydrate utilization pathways (columns) reconstructed in 263 reference *Bifidobacterium* genomes (rows). Full names of abbreviations are provided in Supplementary Table 5. The annotation rows at the bottom represent pathway/phenotype classifications. The annotation column on the right denotes taxonomic groupings. Lines point to specific strains discussed in the text.

Supplementary Fig. 4. **Growth curves of 30 *Bifidobacterium* strains in MRS-AC medium supplemented with different substrates.** Data represent the mean and 95% confidence interval from three replicates (two for some substrates). Labels indicate the substrates used in each

growth assay (see Supplementary Table 15 **for details**). "No substrate" refers to incubation in MRS-AC without added substrate (negative control). Red lines indicate the "no growth" threshold (10% of the maximum OD_{600} observed for a given strain across all substrates), while orange lines mark the "weak growth" threshold (25% of the maximum OD_{600}).

Supplementary Fig. 5. **Reconstructed human milk oligosaccharide (HMO) utilization pathways in *Bifidobacterium* strains.** Pathways were inferred based on the integration of genomic predictions with growth phenotypes and HMO glycoprofiling data.

Supplementary tables

Supplementary Table 1. Distribution of 3,083 *Bifidobacterium* genomes by taxonomic group and geographic origin.

Supplementary Table 2. Metadata for 263 reference Bifidobacterium genomes used in curated metabolic reconstruction.

Supplementary Table 3. Metadata for 2,820 additional *Bifidobacterium* genomes used in the automated pathway prediction pipeline.

Supplementary Table 4. Curated list of functional roles comprising carbohydrate utilization pathways.

Supplementary Table 5. Glossary of reconstructed carbohydrate utilization pathways, associated substrates, and predicted metabolic phenotypes.

Supplementary Table 6. Genomic signatures used to assign pathway variants and predicted binary utilization phenotypes.

Supplementary Table 7. Binary Phenotype Matrix (BPM) depicting 68 carbohydrate utilization pathways reconstructed in 263 reference *Bifidobacterium* genomes.

Supplementary Table 8. Representation of functional roles comprising carbohydrate utilization pathways in 263 reference *Bifidobacterium* genomes.

Supplementary Table 9. Binary Phenotype Matrix (BPM) depicting 68 carbohydrate utilization pathways reconstructed in 2,820 additional *Bifidobacterium* genomes.

Supplementary Table 10. Representation of functional roles comprising carbohydrate utilization pathways in 2,820 additional *Bifidobacterium* genomes.

Supplementary Table 11. Binary Phenotype Matrix (BPM) depicting 30 additional metabolic pathways reconstructed in 3,083 *Bifidobacterium* genomes.

Supplementary Table 12. List of genes used to construct the phylogenetic tree of 263 reference *Bifidobacterium* genomes.

Supplementary Table 13. Comparison of manually curated and automated (Prokka, EggNOG-mapper) annotations for 263 reference *Bifidobacterium* genomes.

Supplementary Table 14. Pathway enrichment analysis.

Supplementary Table 15. List of substrates used in *in vitro* growth experiments.

Supplementary Table 16. Raw *in vitro* growth data for 30 *Bifidobacterium* strains.

Supplementary Table 17. Comparison between predicted carbohydrate utilization phenotypes and *in vitro* growth data.

Supplementary Table 18. Human milk oligosaccharide (HMO) utilization by *Bifidobacterium* strains.

Supplementary Table 19. Reconstructed regulons of transcription factors and their predicted operator sequences

Supplementary Table 20. Custom probes used to deplete *Bc. kashiwanohense* Bg42221_1E1 rRNA.

Supplementary Table 21. Differential gene expression in *Bc. kashiwanohense* Bg42221_1E1 grown on various carbon sources

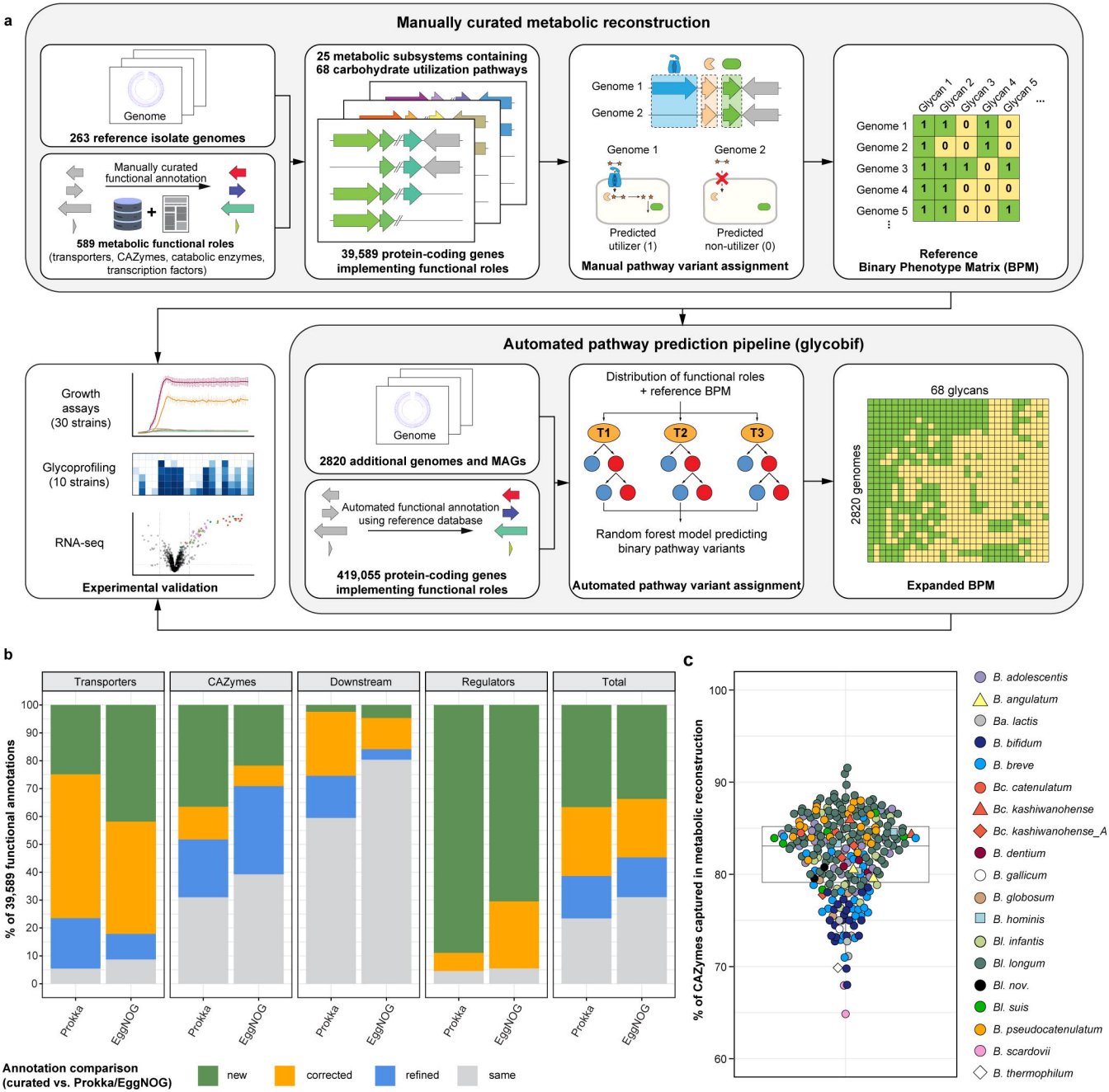
a
Manually curated metabolic reconstruction
Genome
263 reference isolate genomes
Manually curated functional annotation
589 metabolic functional roles
(transporters, CAZymes, catabolic enzymes, transcription factors)
25 metabolic subsystems containing 68 carbohydrate utilization pathways
39,589 protein-coding genes implementing functional roles
Genome 1
Genome 2
Predicted utilizer (1)
Predicted non-utilizer (0)
Manual pathway variant assignment
Glycan 1
Glycan 2
Glycan 3
Glycan 4
Glycan 5
Reference Binary Phenotype Matrix (BPM)
Growth assays (30 strains)
Glycoprofiling (10 strains)
RNA-seq
Experimental validation
Automated pathway prediction pipeline (glycobif)
2820 additional genomes and MAGs
Automated functional annotation using reference database
419,055 protein-coding genes implementing functional roles
Distribution of functional roles + reference BPM
T1
T2
T3
Random forest model predicting binary pathway variants
Automated pathway variant assignment
68 glycans
2820 genomes
Expanded BPM
b
Transporters
CAZymes
Downstream
Regulators
Total
% of 39,589 functional annotations
Prokka
EggNOG
Annotation comparison (curated vs. Prokka/EggNOG)
new
corrected
refined
same
c
% of CAZymes captured in metabolic reconstruction
B. adolescentis
B. angulatum
Ba. lactis
B. bifidum
B. breve
Bc. catenulatum
Bc. kashiwanohense
Bc. kashiwanohense_A
B. dentium
B. gallicum
B. globosum
B. hominis
Bl. infantis
Bl. longum
Bl. nov.
Bl. suis
B. pseudocatenulatum
B. scardovii
B. thermophilum

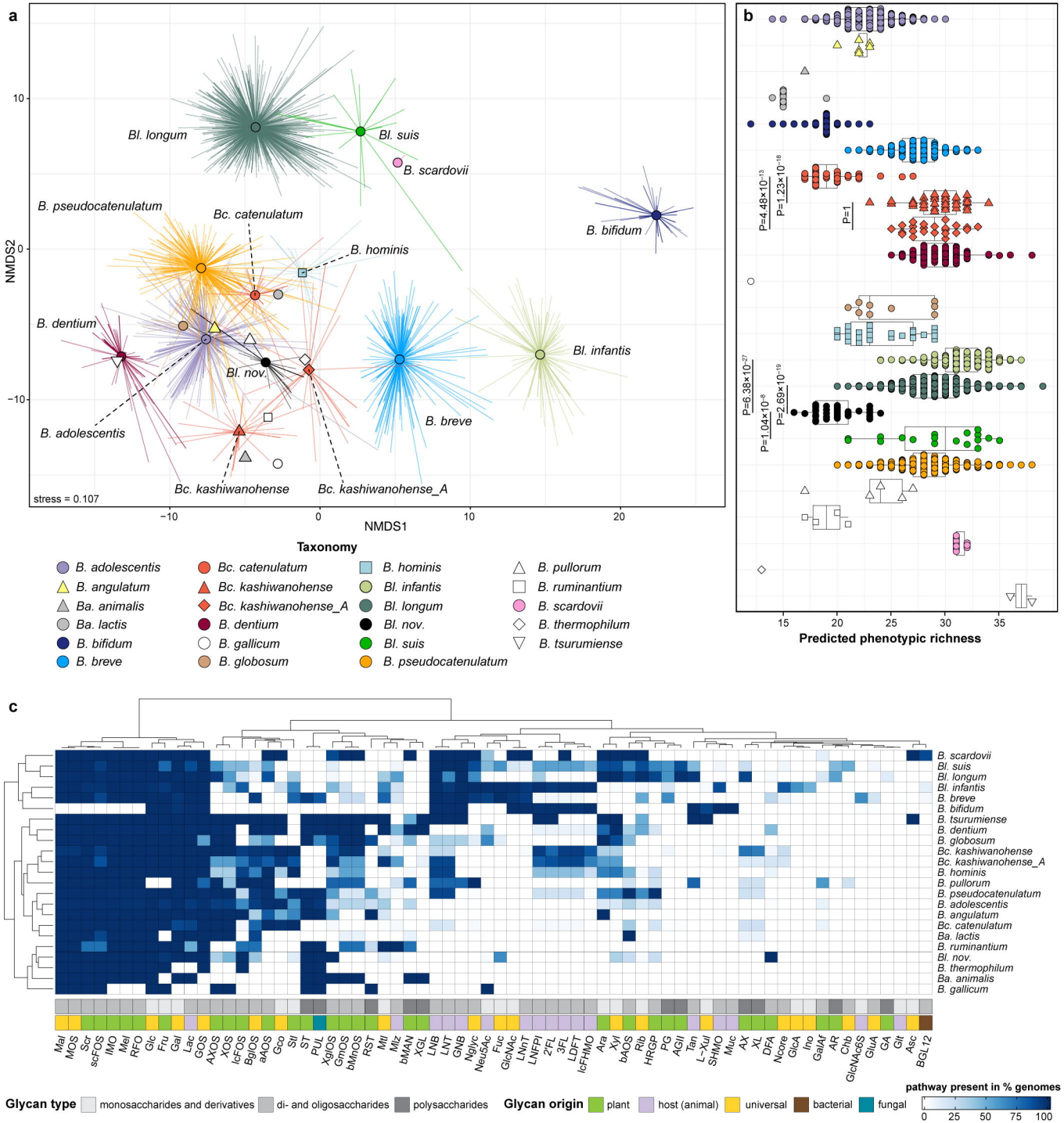
a
Bl. longum
Bl. suis
B. scardovii
B. bifidum
B. pseudocatenulatum
Bc. catenulatum
B. hominis
B. dentium
Bl. nov.
Bl. infantis
B. breve
B. adolescentis
Bc. kashiwanohense
Bc. kashiwanohense_A
stress = 0.107
NMDS1
NMDS2
Taxonomy
B. adolescentis
B. angulatum
Ba. animalis
Ba. lactis
B. bifidum
B. breve
Bc. catenulatum
Bc. kashiwanohense
Bc. kashiwanohense_A
B. dentium
B. gallicum
B. globosum
B. hominis
Bl. infantis
Bl. longum
Bl. nov.
Bl. suis
B. pseudocatenulatum
B. pullorum
B. ruminantium
B. scardovii
B. thermophilum
B. tsurumiense
b
P=4.48×10^-13
P=1.23×10^-18
P=1
P=6.38×10^-27
P=1.04×10^-8
P=2.69×10^-19
Predicted phenotypic richness
c
B. scardovii
Bl. suis
Bl. longum
Bl. infantis
B. breve
B. bifidum
B. tsurumiense
B. dentium
B. globosum
Bc. kashiwanohense
Bc. kashiwanohense_A
B. hominis
B. pullorum
B. pseudocatenulatum
B. adolescentis
B. angulatum
Bc. catenulatum
Ba. lactis
B. ruminantium
Bl. nov.
B. thermophilum
Ba. animalis
B. gallicum
Mal MOS Scr scFOS MIO Mel RFO Glc Fru Gal Lac GOS AXOS XOS IcFOS BglOS aAOS Gco Stl ST PUL XglOS GmOS bMnOS RST Mtl Mtz bMAN XGL LNB LNT GNB Nglyc Neu5Ac Fuc GlcNAc LNnT LNFPI 2'FL 3FL LDFT IcFHMO Ara Xyl bAOS Rib HRGP PG AGII Tan L-Xul SHMO Muc AX XL DFA Ncore GlcA Ino GalAf AR Chb GlcNAc6S GluA GA Glt Asc BGL12
Glycan type
monosaccharides and derivatives
di- and oligosaccharides
polysaccharides
Glycan origin
plant
host (animal)
universal
bacterial
fungal
pathway present in % genomes
0 25 50 75 100

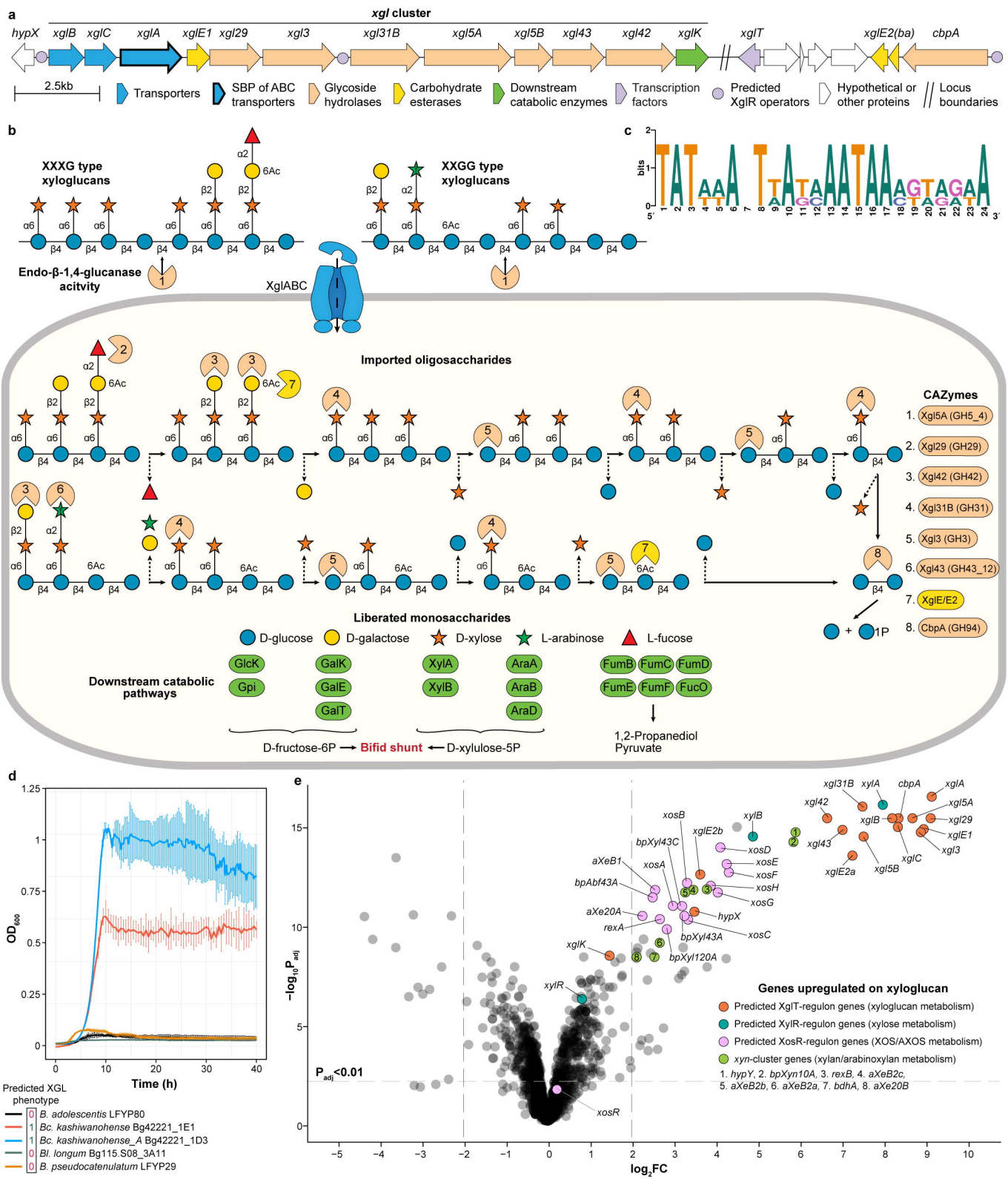
a
xgl cluster
hypX
xglB
xglC
xglA
xglE1
xgl29
xgl3
xgl31B
xgl5A
xgl5B
xgl43
xgl42
xglK
xglT
xglE2(ba)
cbpA
2.5kb
Transporters
SBP of ABC transporters
Glycoside hydrolases
Carbohydrate esterases
Downstream catabolic enzymes
Transcription factors
Predicted XglR operators
Hypothetical or other proteins
Locus boundaries
b
XXXG type xyloglucans
XXGG type xyloglucans
Endo-β-1,4-glucanase acitvity
XglABC
Imported oligosaccharides
CAZymes
1. Xgl5A (GH5_4)
2. Xgl29 (GH29)
3. Xgl42 (GH42)
4. Xgl31B (GH31)
5. Xgl3 (GH3)
6. Xgl43 (GH43_12)
7. XglE/E2
8. CbpA (GH94)
Liberated monosaccharides
D-glucose
D-galactose
D-xylose
L-arabinose
L-fucose
Downstream catabolic pathways
GlcK
Gpi
GalK
GalE
GalT
XylA
XylB
AraA
AraB
AraD
FumB
FumC
FumD
FumE
FumF
FucO
D-fructose-6P
Bifid shunt
D-xylulose-5P
1,2-Propanediol
Pyruvate
c
d
OD600
Time (h)
Predicted XGL phenotype
B. adolescentis LFYP80
Bc. kashiwanohense Bg42221_1E1
Bc. kashiwanohense_A Bg42221_1D3
Bl. longum Bg115.S08_3A11
B. pseudocatenulatum LFYP29
e
−log10 Padj
log2FC
Padj<0.01
Genes upregulated on xyloglucan
Predicted XglT-regulon genes (xyloglucan metabolism)
Predicted XylR-regulon genes (xylose metabolism)
Predicted XosR-regulon genes (XOS/AXOS metabolism)
xyn-cluster genes (xylan/arabinoxylan metabolism)
1. hypY, 2. bpXyn10A, 3. rexB, 4. aXeB2c,
5. aXeB2b, 6. aXeB2a, 7. bdhA, 8. aXe20B

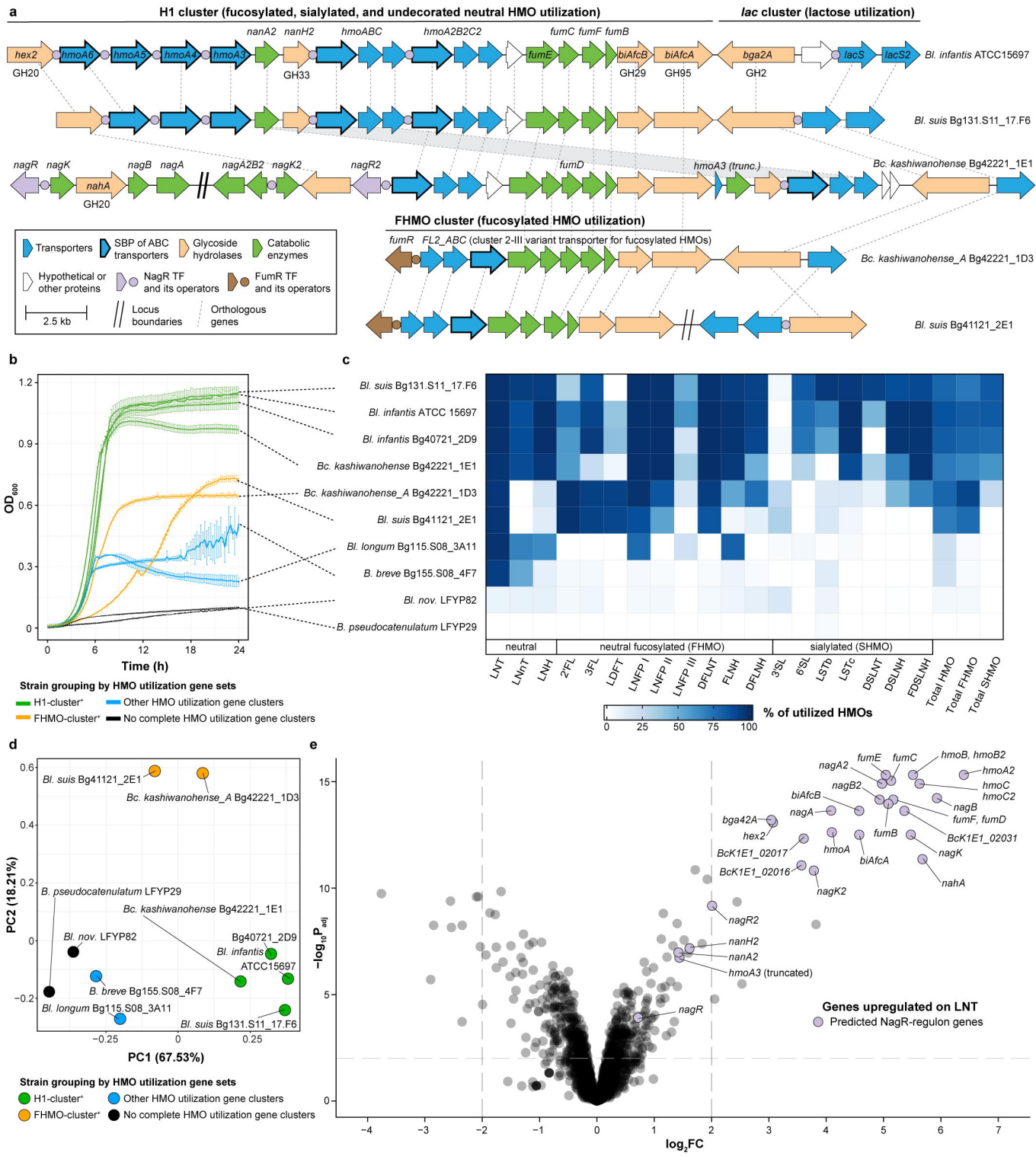
a
H1 cluster (fucosylated, sialylated, and undecorated neutral HMO utilization)
lac cluster (lactose utilization)
hex2
GH20
hmoA6
hmoA5
hmoA4
hmoA3
nanA2
nanH2
GH33
hmoABC
hmoA2B2C2
fumC
fumF
fumB
fumE
biAfcB
GH29
biAfcA
GH95
bga2A
GH2
lacS
lacS2
Bl. infantis ATCC15697
Bl. suis Bg131.S11_17.F6
nagR
nagK
nahA
GH20
nagB
nagA
nagA2B2
nagK2
nagR2
fumD
hmoA3 (trunc.)
Bc. kashiwanohense Bg42221_1E1
FHMO cluster (fucosylated HMO utilization)
fumR
FL2_ABC (cluster 2-III variant transporter for fucosylated HMOs)
Bc. kashiwanohense_A Bg42221_1D3
Bl. suis Bg41121_2E1
Transporters
SBP of ABC transporters
Glycoside hydrolases
Catabolic enzymes
Hypothetical or other proteins
NagR TF and its operators
FumR TF and its operators
2.5 kb
Locus boundaries
Orthologous genes
b
OD600
Time (h)
Strain grouping by HMO utilization gene sets
H1-cluster+
Other HMO utilization gene clusters
FHMO-cluster+
No complete HMO utilization gene clusters
c
Bl. suis Bg131.S11_17.F6
Bl. infantis ATCC 15697
Bl. infantis Bg40721_2D9
Bc. kashiwanohense Bg42221_1E1
Bc. kashiwanohense_A Bg42221_1D3
Bl. suis Bg41121_2E1
Bl. longum Bg115.S08_3A11
B. breve Bg155.S08_4F7
Bl. nov. LFYP82
B. pseudocatenulatum LFYP29
neutral
neutral fucosylated (FHMO)
sialylated (SHMO)
LNT
LNnT
LNH
2'FL
3FL
LDFT
LNFP I
LNFP II
LNFP III
DFLNT
FLNH
DFLNH
3'SL
6'SL
LSTb
LSTc
DSLNT
DSLNH
FDSLNH
Total HMO
Total FHMO
Total SHMO
% of utilized HMOs
d
PC2 (18.21%)
PC1 (67.53%)
Bl. suis Bg41121_2E1
Bc. kashiwanohense_A Bg42221_1D3
B. pseudocatenulatum LFYP29
Bc. kashiwanohense Bg42221_1E1
Bl. nov. LFYP82
Bg40721_2D9
Bl. infantis ATCC15697
B. breve Bg155.S08_4F7
Bl. longum Bg115.S08_3A11
Bl. suis Bg131.S11_17.F6
Strain grouping by HMO utilization gene sets
H1-cluster+
Other HMO utilization gene clusters
FHMO-cluster+
No complete HMO utilization gene clusters
e
−log10 Padj
log2FC
nagA2
fumE
fumC
hmoB, hmoB2
hmoA2
nagB2
hmoC
hmoC2
biAfcB
nagB
nagA
fumF, fumD
bga42A
BcK1E1_02031
hex2
fumB
BcK1E1_02017
hmoA
nagK
biAfcA
BcK1E1_02016
nahA
nagK2
nagR2
nanH2
nanA2
hmoA3 (truncated)
nagR
Genes upregulated on LNT
Predicted NagR-regulon genes

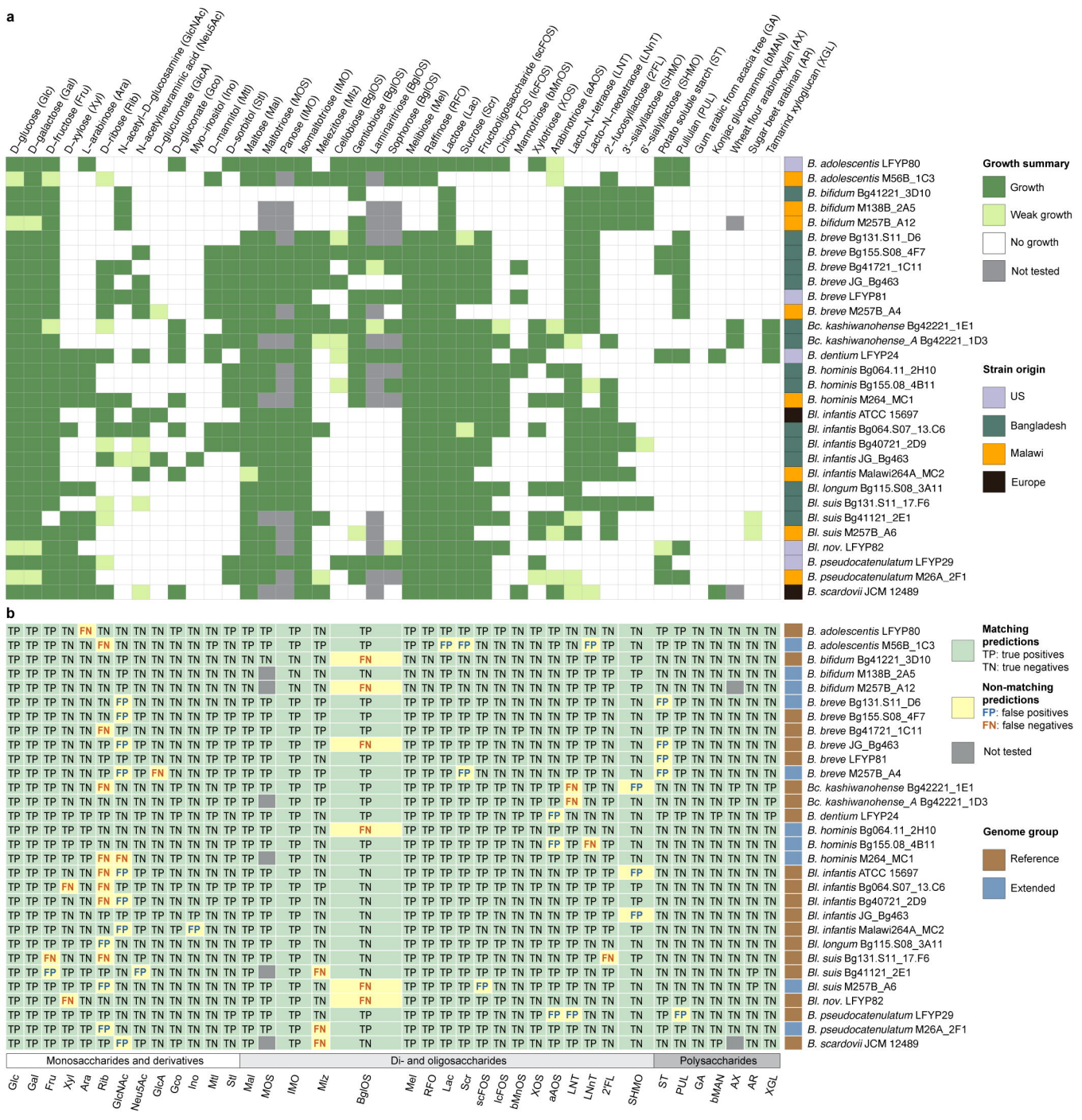
a
D-glucose (Glc)
D-galactose (Gal)
D-fructose (Fru)
D-xylose (Xyl)
L-arabinose (Ara)
D-ribose (Rib)
N-acetyl-D-glucosamine (GlcNAc)
N-acetylneuraminic acid (Neu5Ac)
D-glucuronate (GlcA)
D-gluconate (Gco)
Myo-inositol (Ino)
D-mannitol (Mtl)
D-sorbitol (Stl)
Maltose (Mal)
Maltotriose (MOS)
Panose (IMO)
Isomaltotriose (IMO)
Melezitose (Mlz)
Cellobiose (BglOS)
Gentiobiose (BglOS)
Laminaritriose (BglOS)
Sophorose (BglOS)
Melibiose (Mel)
Raffinose (RFO)
Lactose (Lac)
Sucrose (Scr)
Fructooligosaccharide (scFOS)
Chicory FOS (icFOS)
Mannotriose (bMnOS)
Xylotriose (XOS)
Arabinotriose (aAOS)
Lacto-N-tetraose (LNT)
Lacto-N-neotetraose (LNnT)
2'-fucosyllactose (2'FL)
3'-sialyllactose (SHMO)
6'-sialyllactose (SHMO)
Potato soluble starch (ST)
Pullulan (PUL)
Gum arabic from acacia tree (GA)
Konjac glucomannan (bMAN)
Wheat flour arabinoxylan (AX)
Sugar beet arabinan (AR)
Tamarind xyloglucan (XGL)
B. adolescentis LFYP80
B. adolescentis M56B_1C3
B. bifidum Bg41221_3D10
B. bifidum M138B_2A5
B. bifidum M257B_A12
B. breve Bg131.S11_D6
B. breve Bg155.S08_4F7
B. breve Bg41721_1C11
B. breve JG_Bg463
B. breve LFYP81
B. breve M257B_A4
Bc. kashiwanohense Bg42221_1E1
Bc. kashiwanohense_A Bg42221_1D3
B. dentium LFYP24
B. hominis Bg064.11_2H10
B. hominis Bg155.08_4B11
B. hominis M264_MC1
Bl. infantis ATCC 15697
Bl. infantis Bg064.S07_13.C6
Bl. infantis Bg40721_2D9
Bl. infantis JG_Bg463
Bl. infantis Malawi264A_MC2
Bl. longum Bg115.S08_3A11
Bl. suis Bg131.S11_17.F6
Bl. suis Bg41121_2E1
Bl. suis M257B_A6
Bl. nov. LFYP82
B. pseudocatenulatum LFYP29
B. pseudocatenulatum M26A_2F1
B. scardovii JCM 12489
Growth summary
Growth
Weak growth
No growth
Not tested
Strain origin
US
Bangladesh
Malawi
Europe
b
Matching predictions
TP: true positives
TN: true negatives
Non-matching predictions
FP: false positives
FN: false negatives
Not tested
Genome group
Reference
Extended
Monosaccharides and derivatives
Di- and oligosaccharides
Polysaccharides
Glc
Gal
Fru
Xyl
Ara
Rib
GlcNAc
Neu5Ac
GlcA
Gco
Ino
Mtl
Stl
Mal
MOS
IMO
Mlz
BglOS
Mel
RFO
Lac
Scr
scFOS
icFOS
bMnOS
XOS
aAOS
LNT
LNnT
2'FL
SHMO
ST
PUL
GA
bMAN
AX
AR
XGL

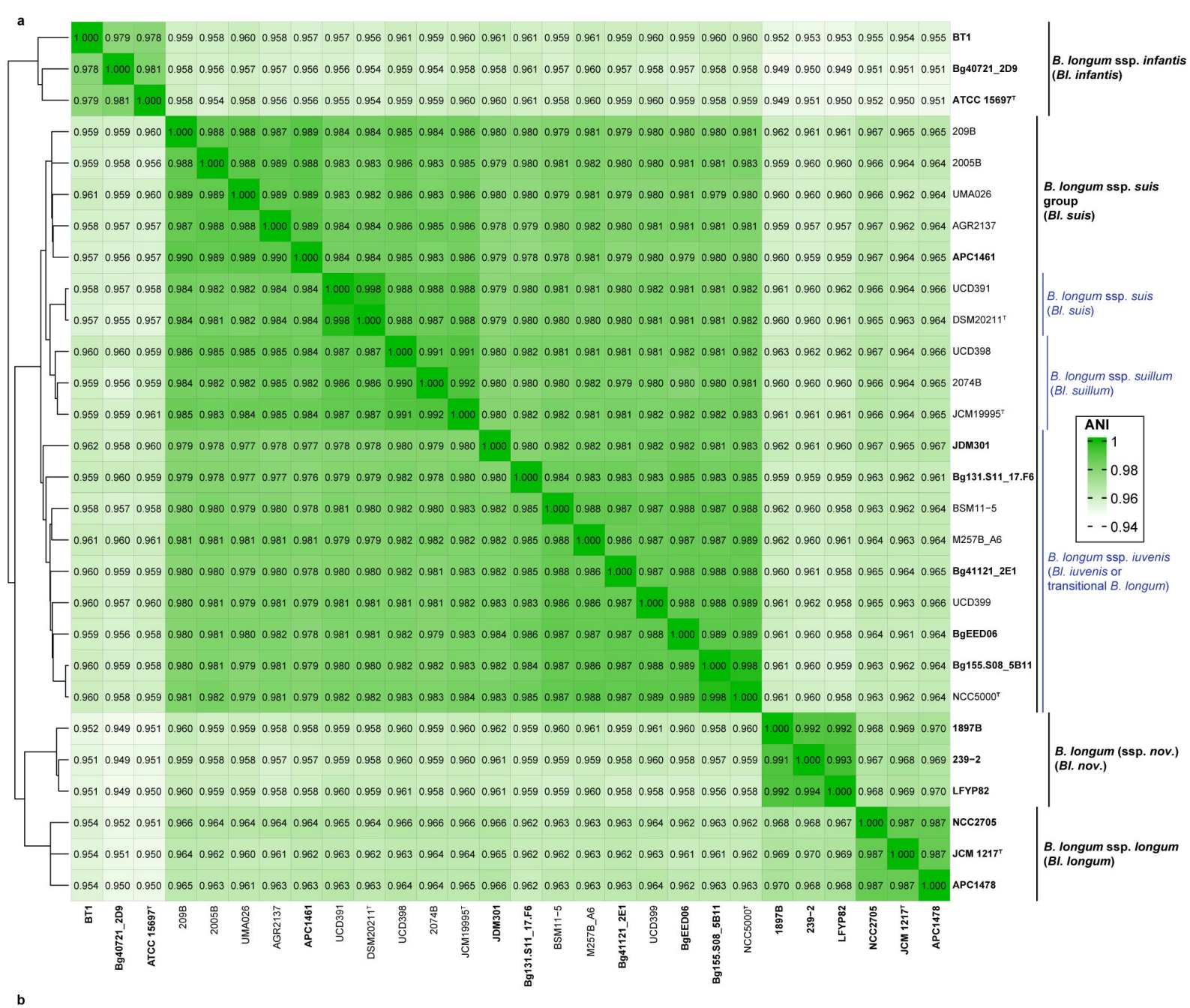
a
BT1
Bg40721_2D9
ATCC 15697T
209B
2005B
UMA026
AGR2137
APC1461
UCD391
DSM20211T
UCD398
2074B
JCM19995T
JDM301
Bg131.S11_17.F6
BSM11-5
M257B_A6
Bg41121_2E1
UCD399
BgEED06
Bg155.S08_5B11
NCC5000T
1897B
239-2
LFYP82
NCC2705
JCM 1217T
APC1478
B. longum ssp. infantis (Bl. infantis)
B. longum ssp. suis group (Bl. suis)
B. longum ssp. suis (Bl. suis)
B. longum ssp. suillum (Bl. suillum)
B. longum ssp. iuvenis (Bl. iuvenis or transitional B. longum)
B. longum (ssp. nov.) (Bl. nov.)
B. longum ssp. longum (Bl. longum)
ANI
1
0.98
0.96
0.94

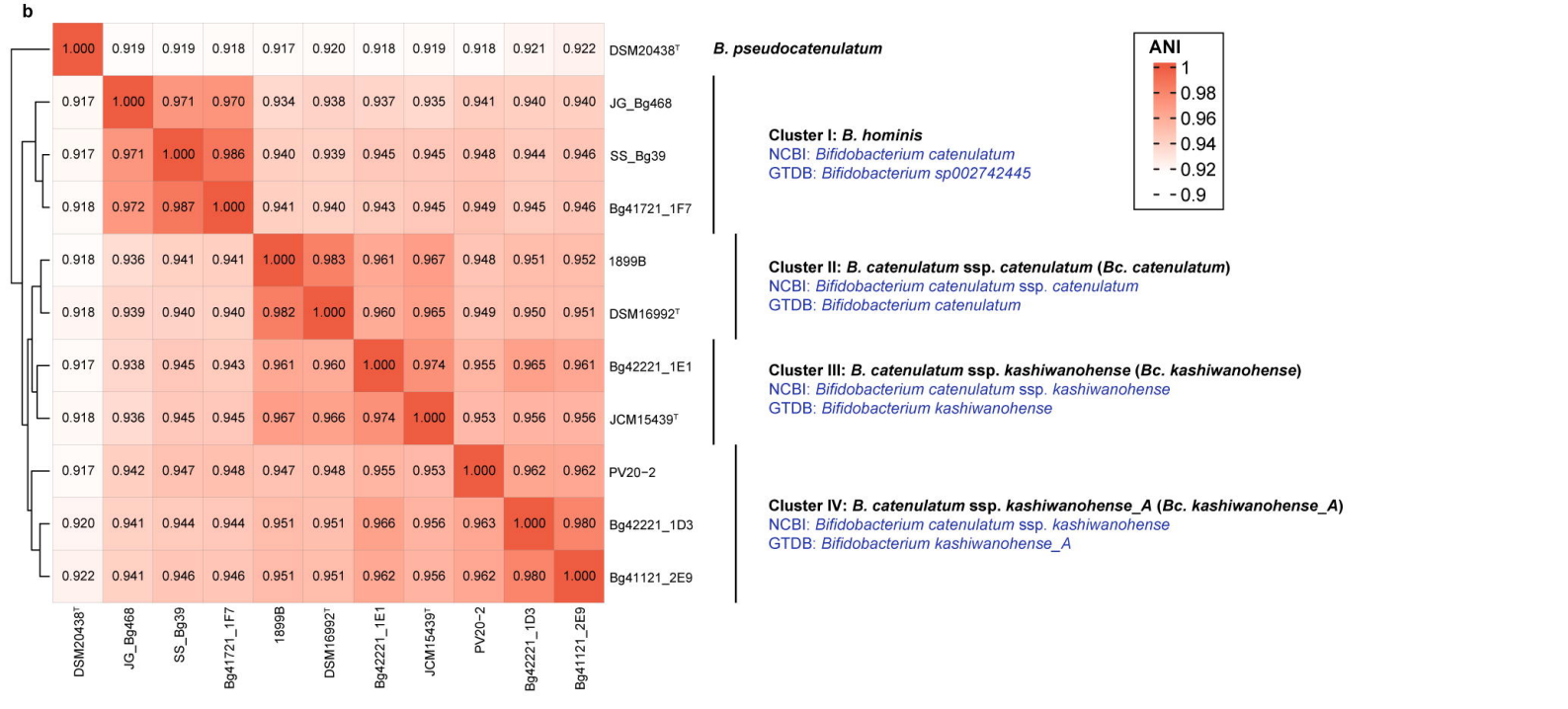
b
DSM20438T
JG_Bg468
SS_Bg39
Bg41721_1F7
1899B
DSM16992T
Bg42221_1E1
JCM15439T
PV20-2
Bg42221_1D3
Bg41121_2E9
B. pseudocatenulatum
Cluster I: B. hominis
NCBI: Bifidobacterium catenulatum
GTDB: Bifidobacterium sp002742445
Cluster II: B. catenulatum ssp. catenulatum (Bc. catenulatum)
NCBI: Bifidobacterium catenulatum ssp. catenulatum
GTDB: Bifidobacterium catenulatum
Cluster III: B. catenulatum ssp. kashiwanohense (Bc. kashiwanohense)
NCBI: Bifidobacterium catenulatum ssp. kashiwanohense
GTDB: Bifidobacterium kashiwanohense
Cluster IV: B. catenulatum ssp. kashiwanohense_A (Bc. kashiwanohense_A)
NCBI: Bifidobacterium catenulatum ssp. kashiwanohense
GTDB: Bifidobacterium kashiwanohense_A
ANI
1
0.98
0.96
0.94
0.92
0.9

(1) Creating a database of *Bifidobacterium* genomes and metabolic functional roles

263 reference *Bifidobacterium* genomes
- 19 species and subspecies
- 19 new genomes of Bangladeshi isolates

25 metabolic subsystems encompassing
- 39,589 protein-coding genes
- 68 carbohydrate utilization pathways

Manually curated list of 589 metabolic functional roles
- 210 characterized in bifidobacteria
- 80 characterized in other taxa
- 143 predicted previously (TCDB, CAZy, KEGG, RegPrecise, publications)
- 156 predicted in this work

222 publications

Glycan transporters (235) | Glycoside hydrolases and other CAZymes (197) | Downstream catabolic enzymes (72) | Transcription factors (85)

(2) Functional gene annotation and reconstruction of carbohydrate utilization pathways

Example: reconstruction of pathways for xylose (Xyl) and xylooligosaccharide (XOS) utilization

***Bl. infantis* R0033**
Gene clusters and regulons
① *xylA* — *xosR* ② *xosA* *xosB* *xosC* *bpXyl43C*
① *xylF* *xylG* *xylH* — *xylB* ① *xylR*

***Bl. infantis* Bg064.S07_13.C6**
Gene clusters and regulons
① *xylA* — *xosR* ② *xosA* *xosB* *xosC* *bpXyl43C*
xylB ① *xylR*

***Bl. infantis* Malawi264A_MC2**
Gene clusters and regulons
xylB (truncated) ① *xylR*

Transporters | Glycoside hydrolases | Downstream catabolic enzymes | Transcription factors | ① ② Predicted XylR and XosR operators

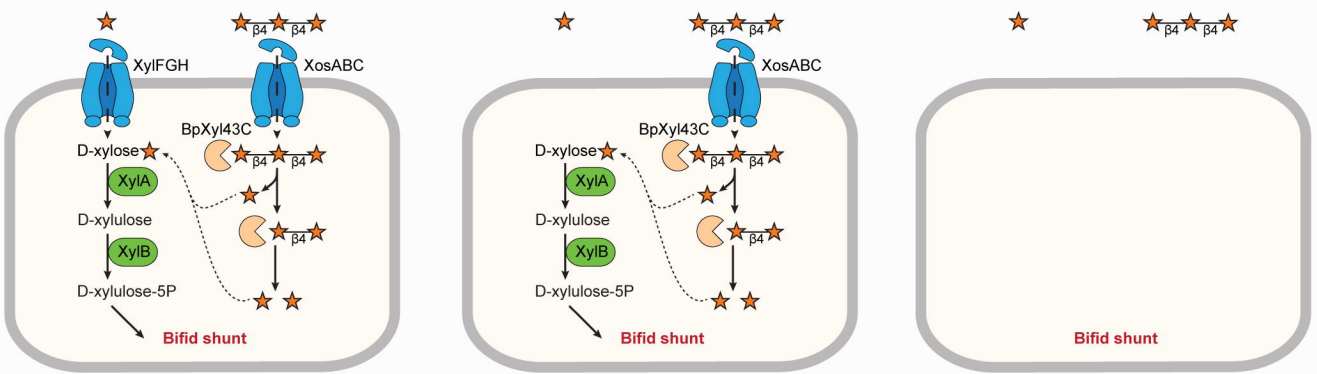

(3) Assignment of pathway variants and binary carbohydrate utilization phenotypes based on genomic signatures

U = transporter + catabolic pathway
Xyl: *xylFGH + xylA + xylB*
XOS: *xosABC + bpXyl43C + xylA + xylB*

P = catabolic pathway only
Xyl: *xylA + xylB*
XOS: *bpXyl43C + xylA + xylB*

N = no catabolic pathway

Pathway variants

Strain	Xyl	XOS
Bl. infantis R0033	U	U
Bl. infantis Bg064.S07_13.C6	P	U
Bl. infantis Malawi264A_MC2	N	N

Conversion to binary phenotypes
U --> 1 (utilizer)
P --> 0 (non-utilizer)
N --> 0 (non-utilizer)

Binary phenotypes

Strain	Xyl	XOS
Bl. infantis R0033	1	1
Bl. infantis Bg064.S07_13.C6	0	1
Bl. infantis Malawi264A_MC2	0	0

Binary Phenotype Matrix (BPM)
263 genomes
68 binary phenotypes

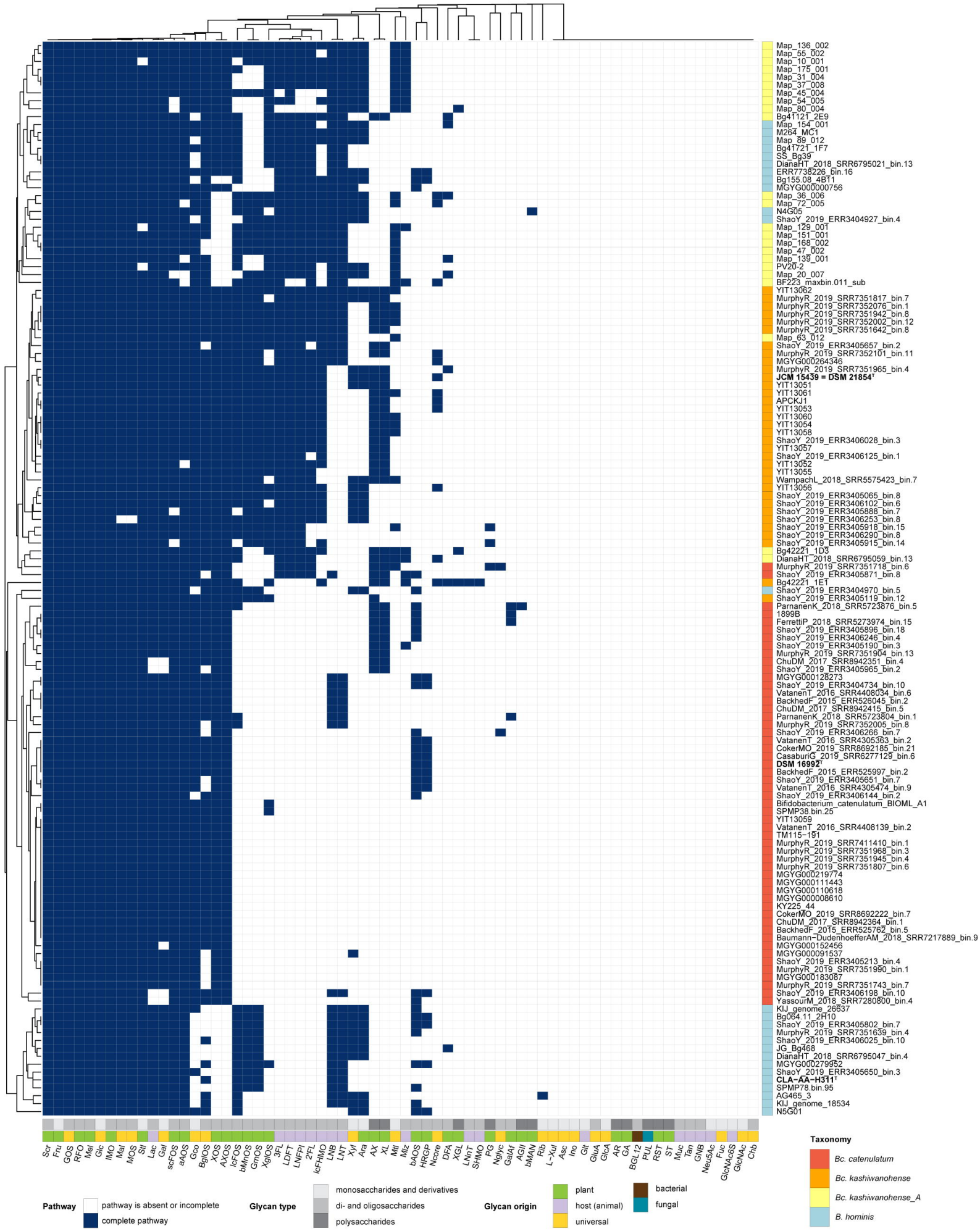
Map_136_002
Map_55_002
Map_10_001
Map_175_001
Map_31_004
Map_37_008
Map_45_004
Map_54_005
Map_80_004
Bg41121_2E9
Map_154_001
M264_MC1
Map_89_012
Bg41721_1F7
SS_Bg39
DianaHT_2018_SRR6795021_bin.13
ERR7738226_bin.16
Bg155.08_4B11
MGYG000000756
Map_36_006
Map_72_005
N4G05
ShaoY_2019_ERR3404927_bin.4
Map_129_001
Map_151_001
Map_168_002
Map_47_002
Map_139_001
PV20-2
Map_20_007
BF223_maxbin.011_sub
YIT13062
MurphyR_2019_SRR7351817_bin.7
MurphyR_2019_SRR7352076_bin.1
MurphyR_2019_SRR7351942_bin.8
MurphyR_2019_SRR7352002_bin.12
MurphyR_2019_SRR7351642_bin.8
Map_63_012
ShaoY_2019_ERR3405657_bin.2
MurphyR_2019_SRR7352101_bin.11
MGYG000264346
MurphyR_2019_SRR7351965_bin.4
JCM 15439 = DSM 21854T
YIT13051
YIT13061
APCKJ1
YIT13053
YIT13060
YIT13054
YIT13058
ShaoY_2019_ERR3406028_bin.3
YIT13057
ShaoY_2019_ERR3406125_bin.1
YIT13052
YIT13055
WampachL_2018_SRR5575423_bin.7
YIT13056
ShaoY_2019_ERR3405065_bin.8
ShaoY_2019_ERR3406102_bin.6
ShaoY_2019_ERR3405888_bin.7
ShaoY_2019_ERR3406253_bin.8
ShaoY_2019_ERR3405918_bin.15
ShaoY_2019_ERR3406290_bin.8
ShaoY_2019_ERR3405915_bin.14
Bg42221_1D3
DianaHT_2018_SRR6795059_bin.13
MurphyR_2019_SRR7351718_bin.6
ShaoY_2019_ERR3405871_bin.8
Bg42221_1E1
ShaoY_2019_ERR3404970_bin.5
ShaoY_2019_ERR3405119_bin.12
ParnanenK_2018_SRR5723876_bin.5
1899B
FerrettiP_2018_SRR5273974_bin.15
ShaoY_2019_ERR3405896_bin.18
ShaoY_2019_ERR3406246_bin.4
ShaoY_2019_ERR3405190_bin.3
MurphyR_2019_SRR7351904_bin.13
ChuDM_2017_SRR8942351_bin.4
ShaoY_2019_ERR3405965_bin.2
MGYG000128273
ShaoY_2019_ERR3404734_bin.10
VatanenT_2016_SRR4408034_bin.6
BackhedF_2015_ERR526045_bin.2
ChuDM_2017_SRR8942415_bin.5
ParnanenK_2018_SRR5723804_bin.1
MurphyR_2019_SRR7352005_bin.8
ShaoY_2019_ERR3406266_bin.7
VatanenT_2016_SRR4305363_bin.2
CokerMO_2019_SRR8692185_bin.21
CasaburiG_2019_SRR6277129_bin.6
DSM 16992T
BackhedF_2015_ERR525997_bin.2
ShaoY_2019_ERR3405651_bin.7
VatanenT_2016_SRR4305474_bin.9
ShaoY_2019_ERR3406144_bin.2
Bifidobacterium_catenulatum_BIOML_A1
SPMP38.bin.25
YIT13059
VatanenT_2016_SRR4408139_bin.2
TM115-191
MurphyR_2019_SRR7411410_bin.1
MurphyR_2019_SRR7351968_bin.3
MurphyR_2019_SRR7351945_bin.4
MurphyR_2019_SRR7351807_bin.6
MGYG000219774
MGYG000111443
MGYG000110618
MGYG000008610
KY225_44
CokerMO_2019_SRR8692222_bin.7
ChuDM_2017_SRR8942364_bin.1
BackhedF_2015_ERR525762_bin.5
Baumann-DudenhoefferAM_2018_SRR7217889_bin.9
MGYG000152456
MGYG000091537
ShaoY_2019_ERR3405213_bin.4
MurphyR_2019_SRR7351990_bin.1
MGYG000183087
MurphyR_2019_SRR7351743_bin.7
ShaoY_2019_ERR3406198_bin.10
YassourM_2018_SRR7280800_bin.4
KIJ_genome_26637
Bg064.11_2H10
ShaoY_2019_ERR3405802_bin.7
MurphyR_2019_SRR7351639_bin.4
ShaoY_2019_ERR3406025_bin.10
JG_Bg468
DianaHT_2018_SRR6795047_bin.4
MGYG000279952
ShaoY_2019_ERR3405650_bin.3
CLA-AA-H311T
SPMP78.bin.95
AG465_3
KIJ_genome_18534
N5G01
Scr
Fru
GOS
RFO
Mel
Glc
IMO
Mal
MOS
Stl
Lac
Gal
scFOS
aAOS
Gco
BglOS
XOS
AXOS
lcFOS
bMnOS
GmOS
XglOS
3FL
LDFT
LNFPI
2'FL
lcFHMO
LNB
LNT
Xyl
Ara
AX
XL
Mtl
Mlz
bAOS
HRGP
Ncore
DFA
XGL
LNnT
SHMO
PG
Nglyc
GalAf
AGII
bMAN
Rib
L-Xul
Asc
Ino
Glt
GluA
GlcA
AR
GA
BGL12
PUL
RST
ST
Muc
Tan
GNB
Neu5Ac
Fuc
GlcNAc6S
GlcNAc
Chb
Taxonomy
Bc. catenulatum
Bc. kashiwanohense
Bc. kashiwanohense_A
B. hominis
Pathway
pathway is absent or incomplete
complete pathway
Glycan type
monosaccharides and derivatives
di- and oligosaccharides
polysaccharides
Glycan origin
plant
host (animal)
universal
bacterial
fungal

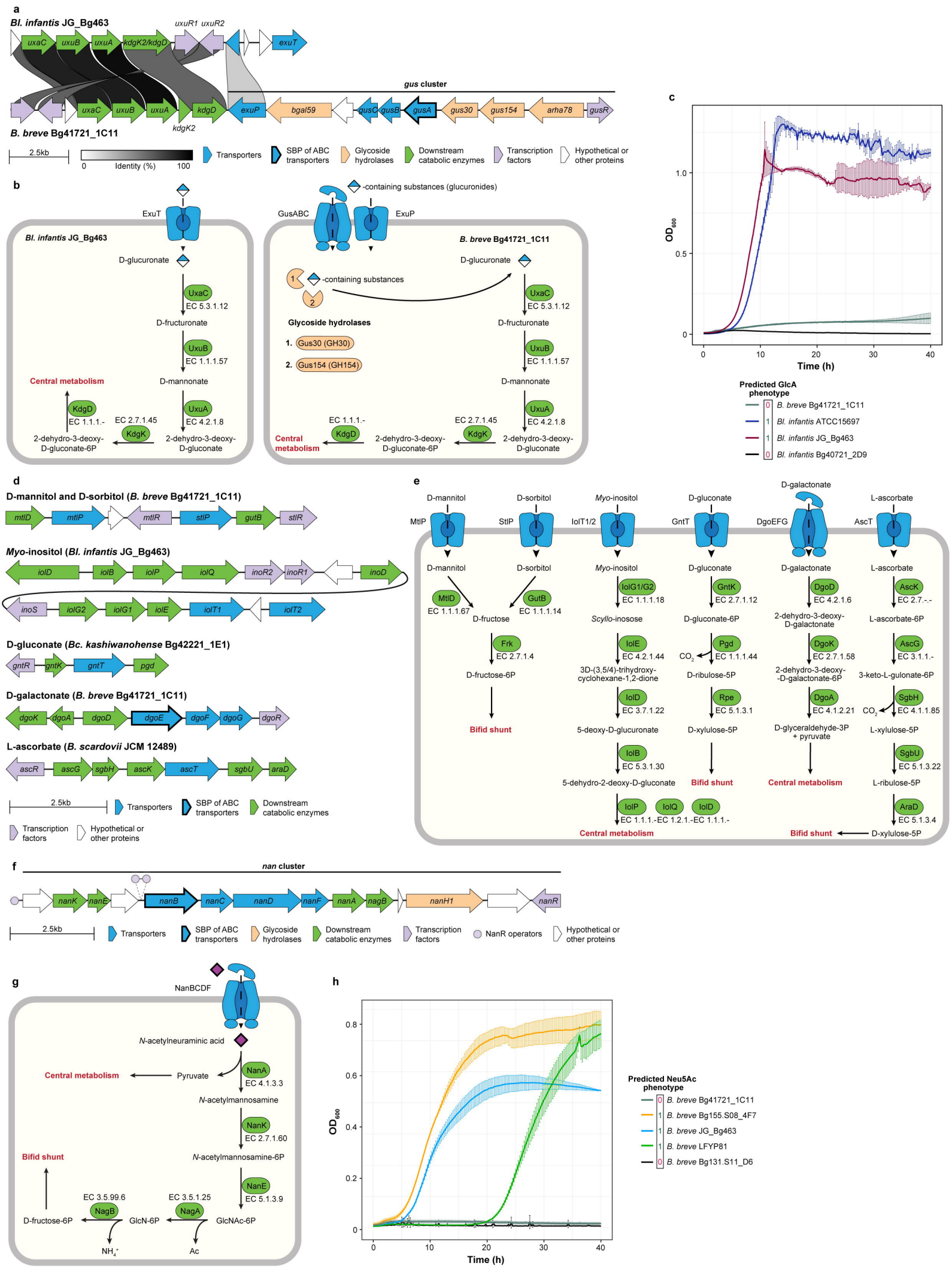
a
Bl. infantis JG_Bg463
uxuR1 uxuR2
uxaC uxuB uxuA kdgK2/kdgD exuT
gus cluster
uxaC uxuB uxuA kdgD exuP bgal59 gusC gusB gusA gus30 gus154 arha78 gusR
kdgK2
B. breve Bg41721_1C11
2.5kb
0 Identity (%) 100
Transporters
SBP of ABC transporters
Glycoside hydrolases
Downstream catabolic enzymes
Transcription factors
Hypothetical or other proteins
b
ExuT
Bl. infantis JG_Bg463
D-glucuronate
UxaC EC 5.3.1.12
D-fructuronate
UxuB EC 1.1.1.57
D-mannonate
UxuA EC 4.2.1.8
2-dehydro-3-deoxy-D-gluconate
EC 2.7.1.45 KdgK
2-dehydro-3-deoxy-D-gluconate-6P
EC 1.1.1.- KdgD
Central metabolism
GusABC
ExuP
-containing substances (glucuronides)
B. breve Bg41721_1C11
-containing substances
Glycoside hydrolases
1. Gus30 (GH30)
2. Gus154 (GH154)
c
OD600
Time (h)
Predicted GlcA phenotype
0 B. breve Bg41721_1C11
1 Bl. infantis ATCC15697
1 Bl. infantis JG_Bg463
0 Bl. infantis Bg40721_2D9
d
D-mannitol and D-sorbitol (B. breve Bg41721_1C11)
mtlD mtlP mtlR stlP gutB stlR
Myo-inositol (Bl. infantis JG_Bg463)
iolD iolB iolP iolQ inoR2 inoR1 inoD
inoS iolG2 iolG1 iolE iolT1 iolT2
D-gluconate (Bc. kashiwanohense Bg42221_1E1)
gntR gntK gntT pgd
D-galactonate (B. breve Bg41721_1C11)
dgoK dgoA dgoD dgoE dgoF dgoG dgoR
L-ascorbate (B. scardovii JCM 12489)
ascR ascG sgbH ascK ascT sgbU araD
2.5kb
Transporters
SBP of ABC transporters
Downstream catabolic enzymes
Transcription factors
Hypothetical or other proteins
e
D-mannitol
D-sorbitol
Myo-inositol
D-gluconate
D-galactonate
L-ascorbate
MtlP StlP IolT1/2 GntT DgoEFG AscT
MtlD EC 1.1.1.67
GutB EC 1.1.1.14
D-fructose
Frk EC 2.7.1.4
D-fructose-6P
Bifid shunt
IolG1/G2 EC 1.1.1.18
Scyllo-inosose
IolE EC 4.2.1.44
3D-(3,5/4)-trihydroxy-cyclohexane-1,2-dione
IolD EC 3.7.1.22
5-deoxy-D-glucuronate
IolB EC 5.3.1.30
5-dehydro-2-deoxy-D-gluconate
IolP IolQ IolD
EC 1.1.1.- EC 1.2.1.- EC 1.1.1.-
Central metabolism
GntK EC 2.7.1.12
D-gluconate-6P
Pgd EC 1.1.1.44
CO2
D-ribulose-5P
Rpe EC 5.1.3.1
D-xylulose-5P
Bifid shunt
DgoD EC 4.2.1.6
2-dehydro-3-deoxy-D-galactonate
DgoK EC 2.7.1.58
2-dehydro-3-deoxy-D-galactonate-6P
DgoA EC 4.1.2.21
D-glyceraldehyde-3P + pyruvate
Central metabolism
AscK EC 2.7.-.-
L-ascorbate-6P
AscG EC 3.1.1.-
3-keto-L-gulonate-6P
SgbH EC 4.1.1.85
CO2
L-xylulose-5P
SgbU EC 5.1.3.22
L-ribulose-5P
AraD EC 5.1.3.4
D-xylulose-5P
Bifid shunt
f
nan cluster
nanK nanE nanB nanC nanD nanF nanA nagB nanH1 nanR
2.5kb
Transporters
SBP of ABC transporters
Glycoside hydrolases
Downstream catabolic enzymes
Transcription factors
NanR operators
Hypothetical or other proteins
g
NanBCDF
N-acetylneuraminic acid
NanA EC 4.1.3.3
Pyruvate
Central metabolism
N-acetylmannosamine
NanK EC 2.7.1.60
N-acetylmannosamine-6P
NanE EC 5.1.3.9
GlcNAc-6P
EC 3.5.1.25 NagA
Ac
GlcN-6P
EC 3.5.99.6 NagB
NH4+
D-fructose-6P
Bifid shunt
h
OD600
Time (h)
Predicted Neu5Ac phenotype
0 B. breve Bg41721_1C11
1 B. breve Bg155.S08_4F7
1 B. breve JG_Bg463
1 B. breve LFYP81
0 B. breve Bg131.S11_D6

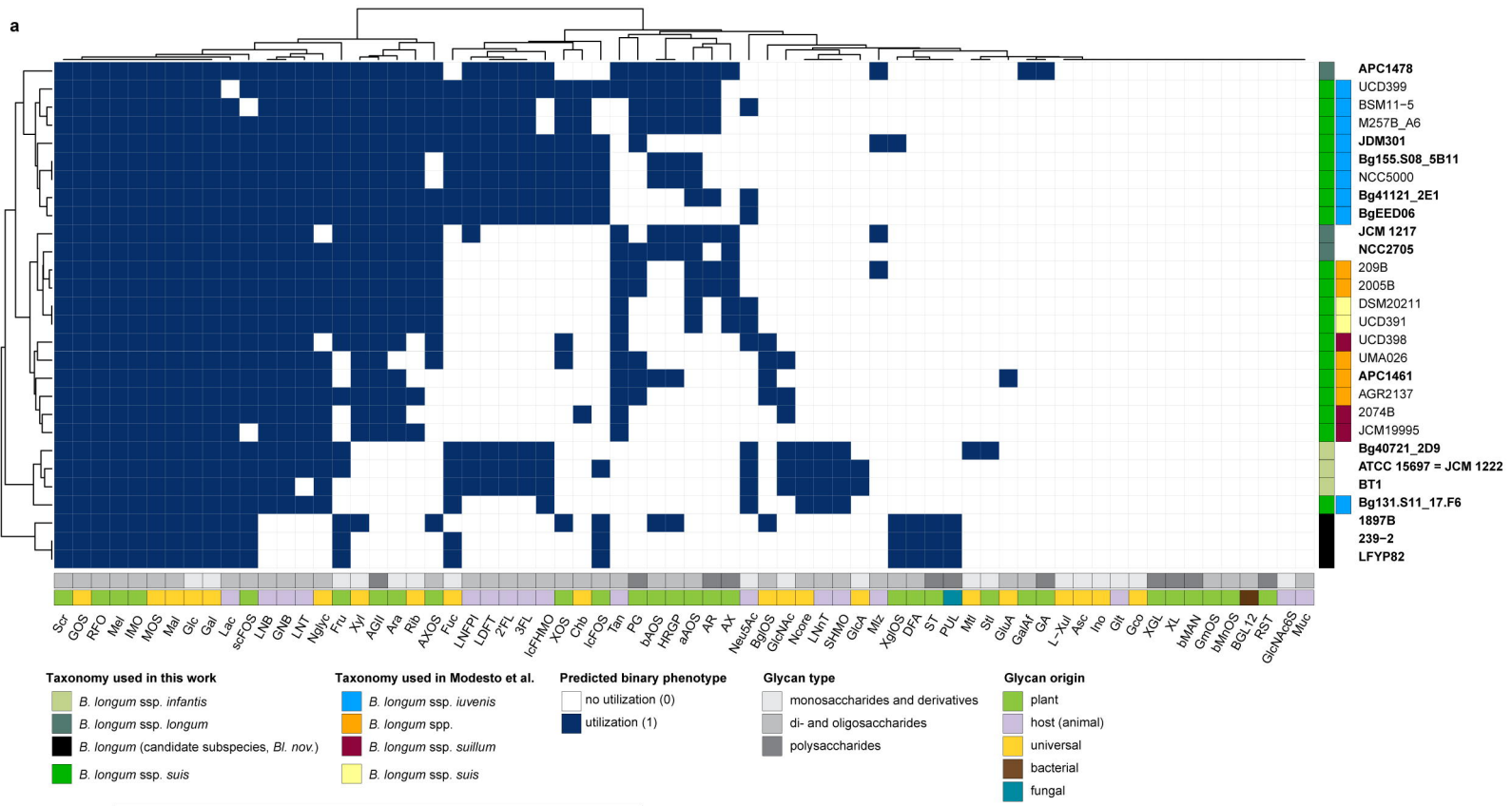
a
APC1478
UCD399
BSM11−5
M257B_A6
JDM301
Bg155.S08_5B11
NCC5000
Bg41121_2E1
BgEED06
JCM 1217
NCC2705
209B
2005B
DSM20211
UCD391
UCD398
UMA026
APC1461
AGR2137
2074B
JCM19995
Bg40721_2D9
ATCC 15697 = JCM 1222
BT1
Bg131.S11_17.F6
1897B
239−2
LFYP82
Scr GOS RFO Mel IMO MOS Mal Glc Gal Lac scFOS LNB GNB LNT Nglyc Fru Xyl AGII Ara Rib AXOS Fuc LNFPI LDFT 2'FL 3FL lcFHMO XOS Chb lcFOS Tan PG bAOS HRGP aAOS AR AX Neu5Ac BglOS GlcNAc Ncore LNnT SHMO GlcA Mtz XglOS DFA ST PUL Mtl Stl GluA GalAf GA L−Xul Asc Ino Glt Gco XGL XL bMAN GmOS bMnOS BGL12 RST GlcNAc6S Muc
Taxonomy used in this work
B. longum ssp. infantis
B. longum ssp. longum
B. longum (candidate subspecies, Bl. nov.)
B. longum ssp. suis
Taxonomy used in Modesto et al.
B. longum ssp. iuvenis
B. longum spp.
B. longum ssp. suillum
B. longum ssp. suis
Predicted binary phenotype
no utilization (0)
utilization (1)
Glycan type
monosaccharides and derivatives
di- and oligosaccharides
polysaccharides
Glycan origin
plant
host (animal)
universal
bacterial
fungal

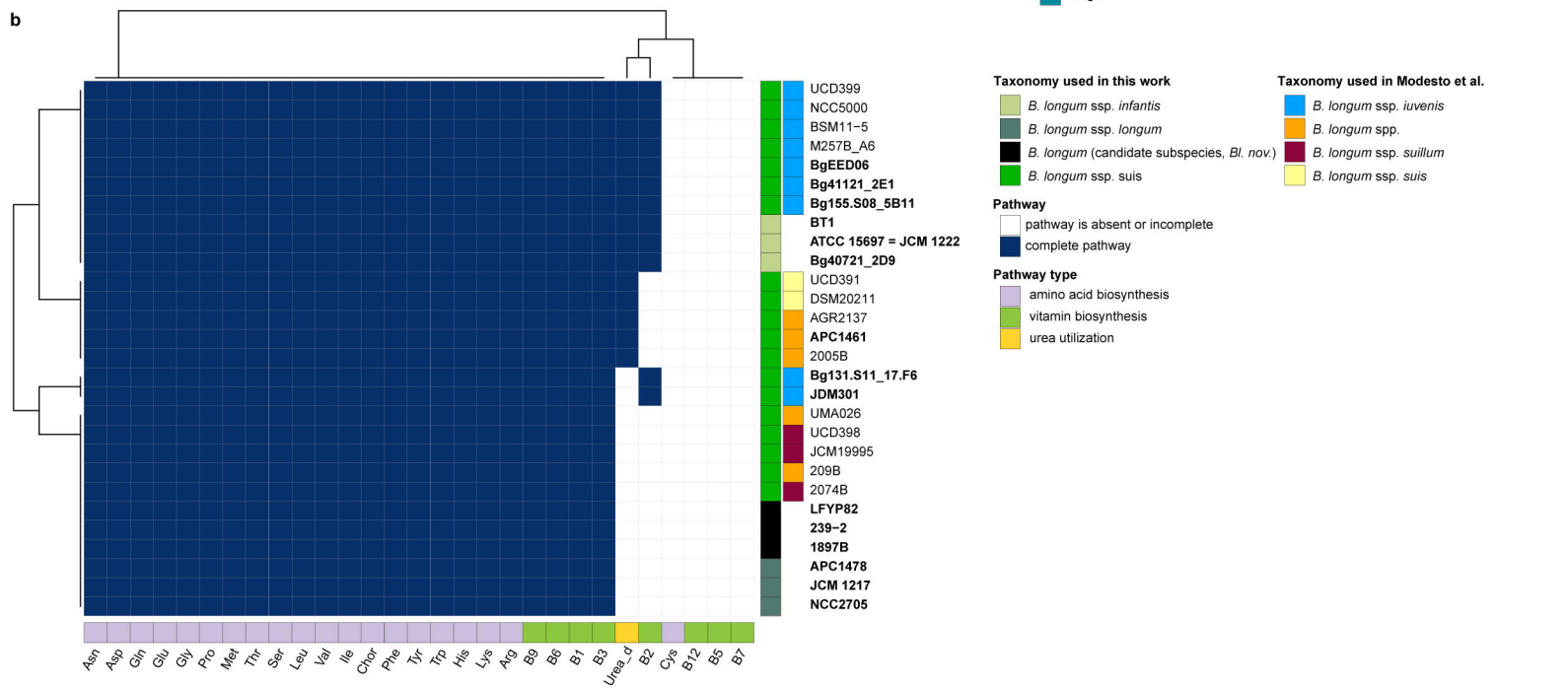
b
UCD399
NCC5000
BSM11−5
M257B_A6
BgEED06
Bg41121_2E1
Bg155.S08_5B11
BT1
ATCC 15697 = JCM 1222
Bg40721_2D9
UCD391
DSM20211
AGR2137
APC1461
2005B
Bg131.S11_17.F6
JDM301
UMA026
UCD398
JCM19995
209B
2074B
LFYP82
239−2
1897B
APC1478
JCM 1217
NCC2705
Asn Asp Gln Glu Gly Pro Met Thr Ser Leu Val Ile Chor Phe Tyr Trp His Lys Arg B9 B6 B1 B3 Urea_d B2 Cys B12 B5 B7
Taxonomy used in this work
B. longum ssp. infantis
B. longum ssp. longum
B. longum (candidate subspecies, Bl. nov.)
B. longum ssp. suis
Taxonomy used in Modesto et al.
B. longum ssp. iuvenis
B. longum spp.
B. longum ssp. suillum
B. longum ssp. suis
Pathway
pathway is absent or incomplete
complete pathway
Pathway type
amino acid biosynthesis
vitamin biosynthesis
urea utilization

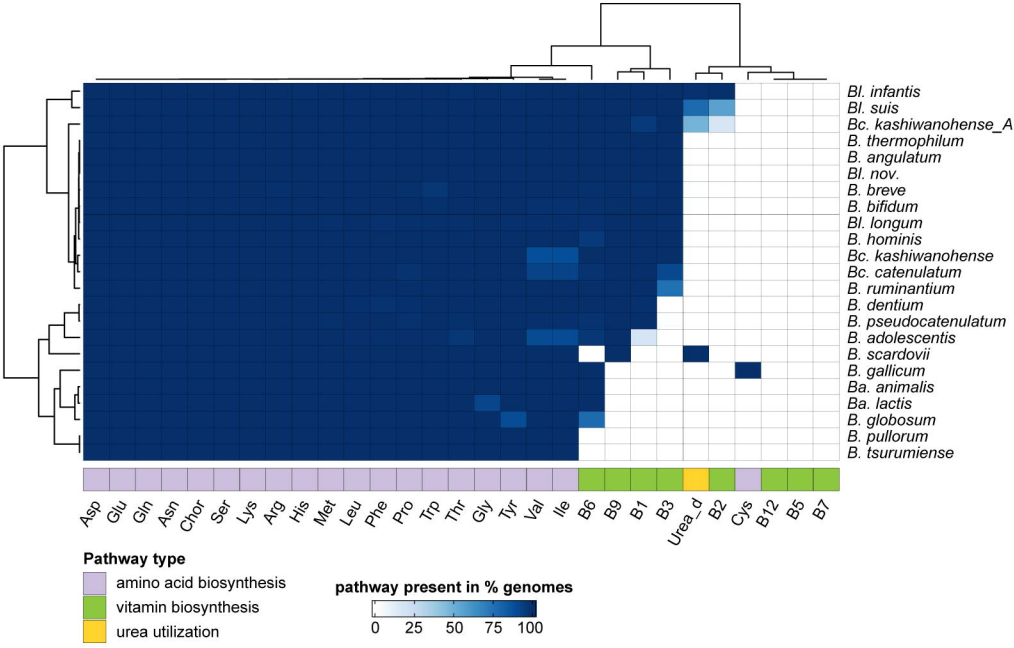
Bl. infantis
Bl. suis
Bc. kashiwanohense_A
B. thermophilum
B. angulatum
Bl. nov.
B. breve
B. bifidum
Bl. longum
B. hominis
Bc. kashiwanohense
Bc. catenulatum
B. ruminantium
B. dentium
B. pseudocatenulatum
B. adolescentis
B. scardovii
B. gallicum
Ba. animalis
Ba. lactis
B. globosum
B. pullorum
B. tsurumiense
Asp
Glu
Gln
Asn
Chor
Ser
Lys
Arg
His
Met
Leu
Phe
Pro
Trp
Thr
Gly
Tyr
Val
Ile
B6
B9
B1
B3
Urea_d
B2
Cys
B12
B5
B7
Pathway type
amino acid biosynthesis
vitamin biosynthesis
urea utilization
pathway present in % genomes
0
25
50
75
100

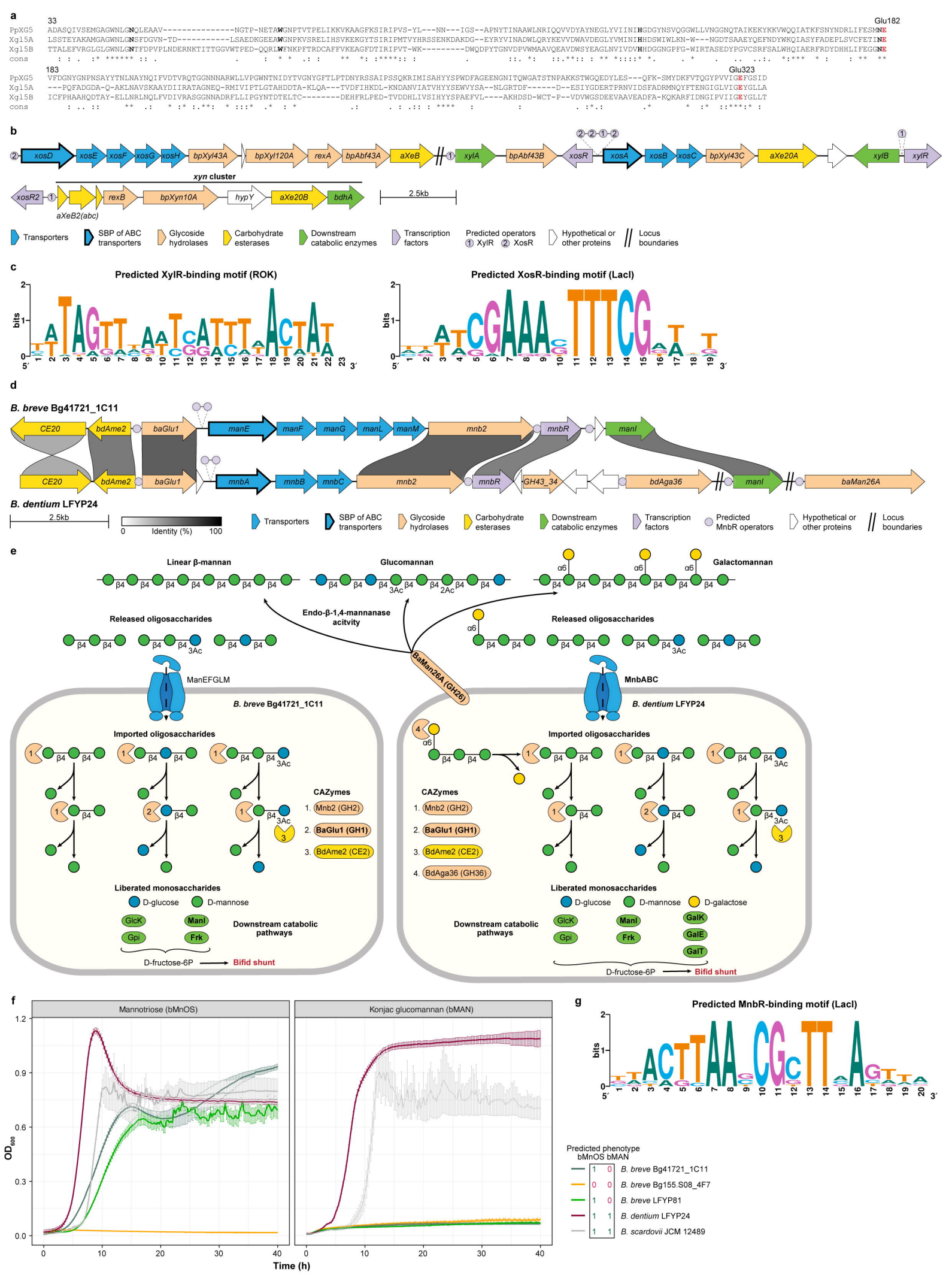
a
33
Glu182
PpXG5 ADASQIVSEMGAGWNLGNQLEAAV----------NGTP-NETAWGNPTVTPELIKKVKAAGFKSIRIPVS-YL---NN---IGS--APNYTINAAWLNRIQQVVDYAYNEGLYVIINIHGDGYNSVQGGWLLVNGGNQTAIKEKYKKVWQQIATKFSNYNDRLIFESMNE
Xg15A LSSTEYAKAMGAGWNLGNSFDGVN-TD----------LSAEDKGEEAWGNPKVSRELIHSVKEKGYTSIRIPMTVYHRSSENKDAKDG--EYRYVINADWLQRYKEVVDWAVDEGLYVMINIHHDSWIWLKN-W---NGDTSAAEYQEFNDYWKQIASYFADEPLSVCFETINE
Xg15B TTALEFVRGLGLGWNLGNTFDPVPLNDERNKTITTGGVWTPED-QQRLWFNKPFTRDCAFFVKEAGFDTIRIPVT-WK---------DWQDPYTGNVDPVWMAAVQEAVDWSYEAGLNVIVDVHHDGGNGPFG-WIRTASEDYPGVCSRFSALWHQIAERFRDYDHHLIFEGGNE
cons : : . :* ***** :: . . : * * .: : ** *: :****:: : . ::. *: ::.**:: : ** *::::* *. . * . .. .:: *:*** * : : ** **
183
Glu323
PpXG5 VFDGNYGNPNSAYYTNLNAYNQIFVDTVRQTGGNNNARWLLVPGWNTNIDYTVGNYGFTLPTDNYRSSAIPSSQKRIMISAHYYSPWDFAGEENGNITQWGATSTNPAKKSTWGQEDYLES---QFK-SMYDKFVTQGYPVVIGEFGSID
Xg15A ---PQFADGDA-Q-AKLNAVSKAAYDIIRATAGNEQ-RMIVIPTLGTAHDDTA-KLQA---TVDFIHKDL-KNDANVIATVHYYSEWVYSA--NLGRTDF------D--ESIYGDERTPRNVIDSFADRMNQYFTENGIGLVIGEYGLLA
Xg15B ICFPHAAHQDTAY-ELLNRLNQLFVDIVRASGGNNADRFLLIPGYNTDTELTC--------DEHFRLPED-TVDDHLIVSIHYYSPAEFVL----AKHDSD-WCT-P--VDVWGSDEEVAAVEADFA-KQKARFIDNGIPVIIGEYGLLT
cons : .. :: ** .: * :* :.**: * :::* .* : * .: . : .:: : **** : : . :*.: .* * :* ::***:* :
b
xosD
xosE
xosF
xosG
xosH
bpXyl43A
bpXyl120A
rexA
bpAbf43A
aXeB
xylA
bpAbf43B
xosR
xosA
xosB
xosC
bpXyl43C
aXe20A
xylB
xylR
xyn cluster
xosR2
rexB
bpXyn10A
hypY
aXe20B
bdhA
aXeB2(abc)
2.5kb
Transporters
SBP of ABC transporters
Glycoside hydrolases
Carbohydrate esterases
Downstream catabolic enzymes
Transcription factors
Predicted operators
XylR
XosR
Hypothetical or other proteins
Locus boundaries
c
Predicted XylR-binding motif (ROK)
Predicted XosR-binding motif (LacI)
bits
5′
3′
d
B. breve Bg41721_1C11
CE20
bdAme2
baGlu1
manE
manF
manG
manL
manM
mnb2
mnbR
manI
mnbA
mnbB
mnbC
GH43_34
bdAga36
baMan26A
B. dentium LFYP24
2.5kb
0
Identity (%)
100
Transporters
SBP of ABC transporters
Glycoside hydrolases
Carbohydrate esterases
Downstream catabolic enzymes
Transcription factors
Predicted MnbR operators
Hypothetical or other proteins
Locus boundaries
e
Linear β-mannan
Glucomannan
Galactomannan
β4
3Ac
2Ac
α6
Endo-β-1,4-mannanase acitvity
Released oligosaccharides
BaMan26A (GH26)
ManEFGLM
MnbABC
B. breve Bg41721_1C11
B. dentium LFYP24
Imported oligosaccharides
CAZymes
1. Mnb2 (GH2)
2. BaGlu1 (GH1)
3. BdAme2 (CE2)
4. BdAga36 (GH36)
Liberated monosaccharides
D-glucose
D-mannose
D-galactose
GlcK
Gpi
ManI
Frk
GalK
GalE
GalT
Downstream catabolic pathways
D-fructose-6P
Bifid shunt
f
Mannotriose (bMnOS)
Konjac glucomannan (bMAN)
OD600
Time (h)
g
Predicted MnbR-binding motif (LacI)
bits
5′
3′
Predicted phenotype
bMnOS bMAN
1 0 B. breve Bg41721_1C11
0 0 B. breve Bg155.S08_4F7
1 0 B. breve LFYP81
1 1 B. dentium LFYP24
1 1 B. scardovii JCM 12489

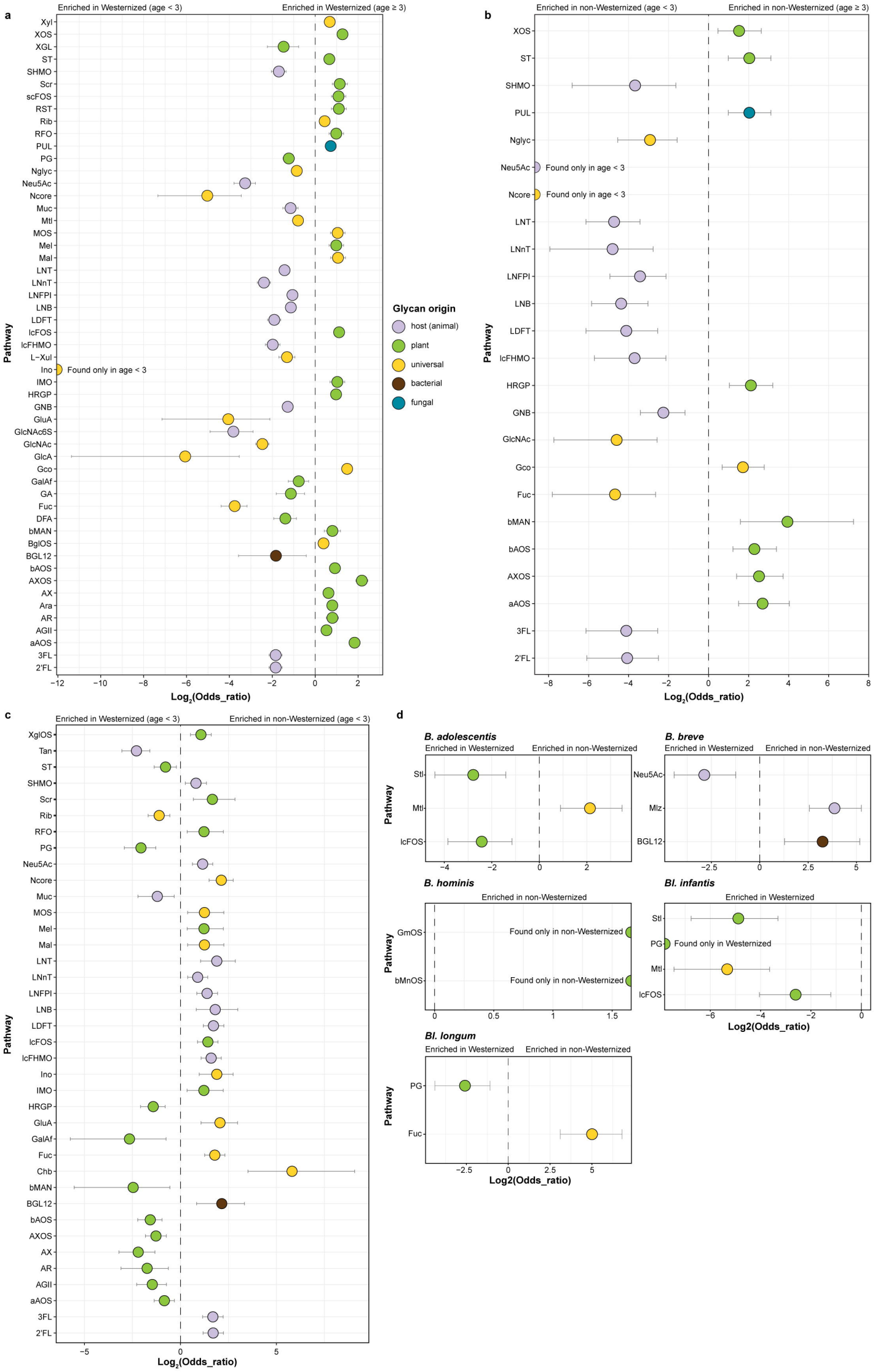
a
Enriched in Westernized (age < 3)
Enriched in Westernized (age ≥ 3)
Pathway
Xyl
XOS
XGL
ST
SHMO
Scr
scFOS
RST
Rib
RFO
PUL
PG
Nglyc
Neu5Ac
Ncore
Muc
Mtl
MOS
Mel
Mal
LNT
LNnT
LNFPI
LNB
LDFT
lcFOS
lcFHMO
L−Xul
Ino
Found only in age < 3
IMO
HRGP
GNB
GluA
GlcNAc6S
GlcNAc
GlcA
Gco
GalAf
GA
Fuc
DFA
bMAN
BglOS
BGL12
bAOS
AXOS
AX
Ara
AR
AGII
aAOS
3FL
2'FL
−12 −10 −8 −6 −4 −2 0 2
Log2(Odds_ratio)
Glycan origin
host (animal)
plant
universal
bacterial
fungal
b
Enriched in non-Westernized (age < 3)
Enriched in non-Westernized (age ≥ 3)
Pathway
XOS
ST
SHMO
PUL
Nglyc
Neu5Ac
Found only in age < 3
Ncore
Found only in age < 3
LNT
LNnT
LNFPI
LNB
LDFT
lcFHMO
HRGP
GNB
GlcNAc
Gco
Fuc
bMAN
bAOS
AXOS
aAOS
3FL
2'FL
−8 −6 −4 −2 0 2 4 6 8
Log2(Odds_ratio)
c
Enriched in Westernized (age < 3)
Enriched in non-Westernized (age < 3)
Pathway
XglOS
Tan
ST
SHMO
Scr
Rib
RFO
PG
Neu5Ac
Ncore
Muc
MOS
Mel
Mal
LNT
LNnT
LNFPI
LNB
LDFT
lcFOS
lcFHMO
Ino
IMO
HRGP
GluA
GalAf
Fuc
Chb
bMAN
BGL12
bAOS
AXOS
AX
AR
AGII
aAOS
3FL
2'FL
−5 0 5
Log2(Odds_ratio)
d
B. adolescentis
Enriched in Westernized
Enriched in non-Westernized
Pathway
Stl
Mtl
lcFOS
−4 −2 0 2
B. breve
Enriched in Westernized
Enriched in non-Westernized
Neu5Ac
Mlz
BGL12
−2.5 0 2.5 5
B. hominis
Enriched in non-Westernized
Pathway
GmOS
Found only in non-Westernized
bMnOS
Found only in non-Westernized
0 0.5 1 1.5
Bl. infantis
Enriched in Westernized
Stl
PG
Found only in Westernized
Mtl
lcFOS
−6 −4 −2 0
Log2(Odds_ratio)
Bl. longum
Enriched in Westernized
Enriched in non-Westernized
Pathway
PG
Fuc
−2.5 0 2.5 5
Log2(Odds_ratio)

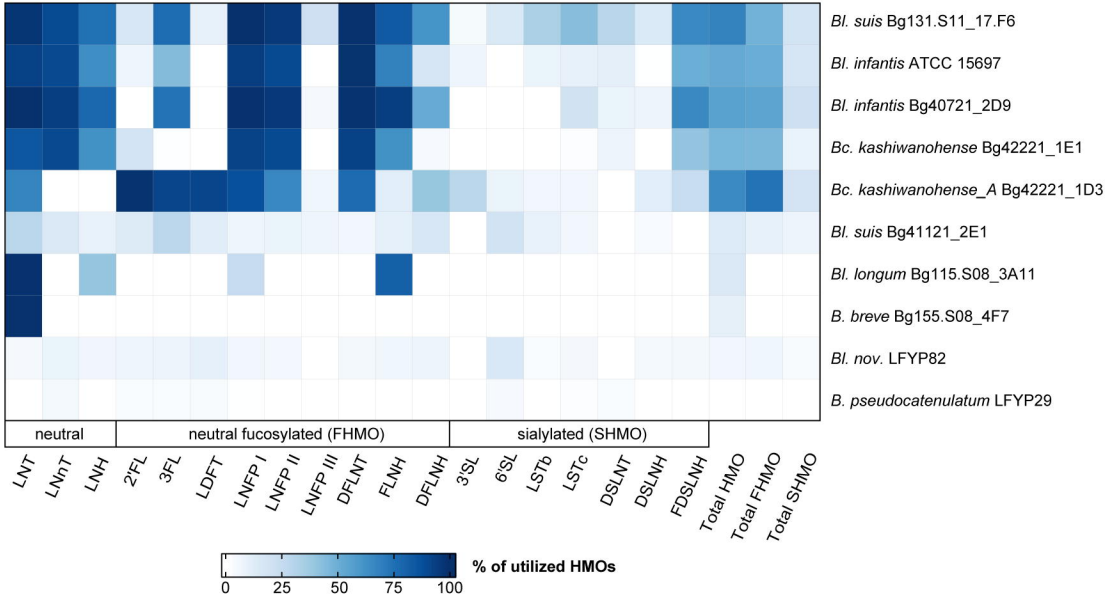
Bl. suis Bg131.S11_17.F6
Bl. infantis ATCC 15697
Bl. infantis Bg40721_2D9
Bc. kashiwanohense Bg42221_1E1
Bc. kashiwanohense_A Bg42221_1D3
Bl. suis Bg41121_2E1
Bl. longum Bg115.S08_3A11
B. breve Bg155.S08_4F7
Bl. nov. LFYP82
B. pseudocatenulatum LFYP29
neutral
neutral fucosylated (FHMO)
sialylated (SHMO)
LNT
LNnT
LNH
2'FL
3FL
LDFT
LNFP I
LNFP II
LNFP III
DFLNT
FLNH
DFLNH
3'SL
6'SL
LSTb
LSTc
DSLNT
DSLNH
FDSLNH
Total HMO
Total FHMO
Total SHMO
% of utilized HMOs
0
25
50
75
100